J. Membrane Biol. 187, 97–115 (2002)
DOI: 10.1007/s00232-001-0155-5

The Journal of
Membrane
Biology

© Springer-Verlag New York Inc. 2002

Na,K-ATPase in the Nuclear Envelope Regulates Na^+: K^+ Gradients in Hepatocyte Nuclei

M.H. Garner
Department of Pathology and Anatomy, UNT Health Science Center, 3500 Camp Bowie Blvd., Fort Worth, TX 76107

Received: 12 July 2001/Revised: 19 December 2001

Abstract. Evidence is emerging that the nuclear envelope itself is responsible for transport and signaling activities quite distinct from those associated with the nuclear pore. For example, the envelope has a Ca^{2+}-signaling pathway that, among other things, regulates meiosis in oocytes. The nuclear envelope's outer membrane also contains K^+ channels. Here we show that Na^+/K^+ gradients exist between the nuclear envelope lumen and both cytoplasm and nucleoplasm in hepatocyte nuclei. The gradients are formed by Na,K-ATPases in the envelope's inner membrane, oriented with the ATP hydrolysis site in the nucleoplasm. We further demonstrate nucleoplasm/cytoplasm Na^+ and K^+ gradients, of which only the Na^+ gradient is dissipated directly by Na,K-ATPase inhibition with ouabain. Finally, our results demonstrate that nuclear pores are not freely permeable to sodium and potassium. Based on these results and numerous in vitro studies, nuclear monovalent cation transporters and channels are likely to play a role in modulation of chromatin structure and gene expression.

Key words: Nuclear envelope — Na,K-ATPase isoforms — Immunocytochemistry — Sodium green-dextran — SBFI-am — PBFI-am

Introduction

Historically, the nuclear pore is not considered restrictive to small cations or anions because of its large internal diameter (Bustamante, Hanover & Liepins, 1995). Nevertheless, a concentration gradient does exist between cytoplasm and nucleoplasm for at least one cation, Ca^{2+} (Lui et al., 1998a; 1998b). To effectively form ion gradients between cytoplasm and nucleoplasm, transport systems must be present in the nuclear envelope to counteract the presumed sizable leak through the nuclear pore (Bustamante et al., 1995). For example, directional transport of Ca^{2+} across the nuclear envelope involves the polarized distribution of Ca^{2+} pumps and Ca^{2+} channels. The Ca^{2+}-ATPase, located in the outer membrane of the nuclear envelope (Lanini, Bachs & Carafoli, 1992; Bachs, Agell & Carafoli, 1994), pumps Ca^{2+} into the nuclear envelope lumen, thus creating lumenal Ca^{2+} stores (Gerasimenko et al., 1996). In the nuclear envelope's inner membrane, inositol trisphosphate-regulated Ca^{2+} channels allow the release of these stores into the nucleoplasm (Gerasimenko et al., 1995; Guihard, Proteau & Rousseau, 1997). While lumenal Ca^{2+} stores may play a role in meiosis (Santella & Kyozuka, 1997), they do not affect nuclear envelope assembly or active import and export of macromolecules (Marshall, Gant & Wilson, 1997; Strubing & Clapham, 1999). The membranes of the nuclear envelope also contain an ATP-dependent iron transport system (Gurgueira & Meneghini, 1996), a K^+/H^+ exchange system (Masuda et al., 1998), Cl^- channels and Ca^{2+}-dependent K^+ channels (Mazzanti et al., 1990; Tabares, Mazzanti & Clapham, 1991; Bustamante, 1992; Maruyama, Shimada & Taniguchi, 1995). The Cl^- and K^+ channels are located in the outer membrane of the nuclear envelope (Mazzanti et al., 1990; Tabares et al., 1991; Bustamante, 1992; Maruyama et al., 1995).

For gradient-dependent ion flux through these nuclear envelope K^+ channels, the lumenal K^+ concentration must be different than that of the cytoplasm. It would then follow that there must be K^+ transport systems to maintain lumenal:cytoplasmic K^+ gradients. In the plasma membrane and in membranes of cellular organelles, ATP-dependent

Corresponding to: M.H. Garner; email: mgarner@hsc.unt.edu

exchange of K^+ for either H^+ or Na^+ is responsible for transmembrane K^+ gradients. For example, the plasma membrane Na,K-ATPase sustains Na^+ and K^+ gradients that regulate homeostatic processes such as maintenance of cell volume, transepithelial transport and membrane potential (Skou & Esmann, 1992). Here, we demonstrate, for the first time, the presence of lumenal:nucleoplasmic and lumenal: cytoplasmic Na^+:K^+ gradients in hepatocyte nuclei. We also show that these gradients are maintained by Na,K-ATPases in the nuclear envelope's inner membrane.

Materials and Methods

Materials

Several faculty members of the Department of Pathology and Anatomy, UNTHSC, supplied rat livers for this study. The human hepatocellular carcinoma cell line, HepG2 (ATCC HB 8065), was obtained from the American Type Culture Collection, Rockville, MD. DAPI, Texas-red™ dextran (TRDX, MW 10,000), sodium-green dextran (SGDX, MW 10,000), SBFI-am, PBFI-am, SBFI, PBFI, pluronic acid and Alexa-green-labeled goat anti-rabbit IgG and Alexa-red-labeled goat anti-mouse IgG were obtained from Molecular Probes, Eugene, OR. ^{86}RbCl and ^{22}NaCl were from Amersham, Piscataway, NJ. Microsomal fractions from rat kidney, heart and brain as well as the following anti-Na,K-ATPase antibodies were from Upstate Biotechnology (Lake Placid, NY): a monoclonal antibody (ID # 05369) specific for the α1 catalytic subunit isoform; polyclonal antibodies, ID # 06520 (α1FP), 06168 (α2FP), and 06172 (α3FP), specific for the α1, α2 and α3 catalytic subunit isoforms, respectively. Monoclonal pan-anti-histone IgG, as well as peroxidase-labeled goat anti-rabbit IgG and goat anti-mouse IgG (hrp-GAR and hrp-GAM, respectively) were from Boehringer Mannheim (lndianapolis, IN). Tissue culture supplies were from Life Technologies, Grand Island, NY; SDS-PAGE supplies were from Bio-Rad (Hercules, CA). Monoclonal anti-splicing factor (S-35) antibody was from Sigma (St. Louis, MO). Unless indicated otherwise, all additional reagents were from Sigma.

Isolation and Characterization of Rat Liver Nuclei

Nuclei were isolated from homogenates of perfused rat livers using previously published procedures (Fleischer & Kervina, 1974). Briefly, the minced livers were homogenized in five volumes/g tissue ice-cold TKM (10 mM, Tris-HCl, pH 7.5, 25 mM KCl, 5 mM $MgCl_2$ and 1 mM dithiothreitol) that contained 250 mM sucrose. The homogenate was filtered through five layers of cheesecloth before centrifugation at 700 × g for 10 minutes at 4°C. The pellet was rehomogenized in an equal volume of ice-cold TKM, filtered through cheesecloth and recentrifuged at 700 × g for 10 minutes. The combined supernatants were centrifuged at 40,000 × g to pellet the microsomal fraction. The pellet from the low-speed centrifugation was suspended in 1.6 M sucrose in TKM (2 volumes per gram tissue). Discontinuous sucrose gradients were prepared (16 ml of the suspended pellet overlayed with 0.32 M sucrose in TKM) in ultraclear tubes for the SW28 rotor (Beckman). The gradients were centrifuged at 23,000 rpm for 70 minutes in the SW-28 rotor. After discarding the supernatant, the pellet was resuspended in 2.0 M sucrose in TKM and centrifuged at 45,000 rpm (Ti 45 rotor, Beckman) for 30 minutes at 4°C. After discarding the supernatant, the brown pellet along the tube side (mitochondria) and the whitish-grey pellet at the tube bottom (nuclei) were each suspended and stored at 4°C, in 10 mM Tris-HCl buffer, pH 7.4, which contained (in mM) 5 $MgCl_2$, 25 KCl, 320 sucrose, 1 dithiothreitol (DTT) and 0.1 phenylmethylsulfonyl fluoride (nuclear storage buffer).

Nuclear fraction purity was determined from UV-vis spectra, slot blot analysis, 5′-nucleotidase-activity measurements and electron microscopy. Absorption spectra between 240 nm and 500 nm were determined using a DU 50 spectrophotometer (Beckman, Fullerton, CA). For the nuclear fraction, there was no absorption at 415 nm (Soret band for the heme of mitochondrial cytochromes) and the ratio $A_{260} : A_{280}$ was ≥ 1.2 due to the presence of nucleic acids. The purity of the nuclear fraction was further tested using slot blots probed with organelle-specific antisera to cytochrome oxidase (Molecular Probes), histone (Boehringer Mannheim), Bip (StressGen, Victoria, B.C., Canada) and Golgi 58K (Sigma) as markers for mitochondria, nuclei, endoplasmic reticulum and Golgi, respectively (Fig. 1*a*). Slot blots were stained using previously described methods (Garner & Kong, 1999). Strong staining was observed with the histone antibody. The weak staining that was observed with antiserum to Bip was expected since the outer membrane of the nuclear envelope is continuous with the endoplasmic reticulum. Occasionally, a preparation contained minor mitochondrial contaminants as evidenced by a weak, positive reaction with the cytochrome oxidase antiserum. To test which subfractions contained plasma membrane, the activity of 5′-nucleotidase, a plasma membrane enzyme, was determined in each subfraction using previously published techniques (Harb et al., 1983; Hubbard, Wall & Ma, 1983; Sehmi, Williams & Williams, 1986). The 5′-nucleotidase activity was then compared to Na,K-ATPase activity in the same subfractions. Na,K-ATPase activity was measured using previously described procedures (Simon et al., 1996). The results for a typical preparation (Table 1) indicate that the 5′-nucleotidase is predominantly found in the microsomal fraction and not in the mitochondrial (*data not included*) or nuclear fractions. The specific activity for Na,K-ATPase is increased two-fold in the microsomal fraction, a result similar to that for 5′-nucleotidase. The specific activity of Na,K-ATPase increased 1.8-fold in the nuclear fraction, a result distinctly different from that for 5′-nucleotidase where the activity in the nuclear fraction was 18% of that in the homogenate. These results indicate that the Na,K-ATPase in the nuclear fraction does not represent plasma membrane contamination but, instead, represents a separate pool of Na,K-ATPase in the hepatocyte.

For electronmicroscopic examination of the nuclear fraction (Fig. 1*b* and *c*), nuclei in storage buffer containing 0.5% bovine serum albumin were pelleted (5000 × g, 1–2 min). The supernatant was removed and replaced with fixative, 0.5 ml of 2.5% glutaraldehyde in storage buffer. After fixation for 5 hours, the fixative was removed and the pellet was washed with storage buffer, post-fixed with OsO_4, stained with uranylacetate and lead citrate, dehydrated, embedded in epon, and sectioned (Fleischer & Kervina, 1974). Sections (0.1 μm, on grids) were studied with a Zeiss 910 transmission microscope, confirming that the preparations were enriched in intact nuclei (Fig. 1*b* and *c*). Using these micrographs and assuming a spherical shape, volumes (mean ± SD, $n = 45$) of 8.6 ± 2.4 (10^{-11}) ml, 0.58 ± 0.12 (10^{-11}) ml and 9.18 ± 2.5 (10^{-11}) ml were obtained for the nucleoplasm, nuclear envelope lumen and nucleus, respectively.

A spectroscopic method for quantifying number of nuclei was developed to minimize exposure to high-energy radiation in experiments using $^{86}Rb^+$ and $^{22}Na^+$. Briefly, nuclei, suspended in storage buffer, were treated with DAPI (Haugland, 1996). Aliquots of stained nuclei were placed on polylysine-coated slides with mounting medium (Fluoromount, Southern Biotechnology Associates,

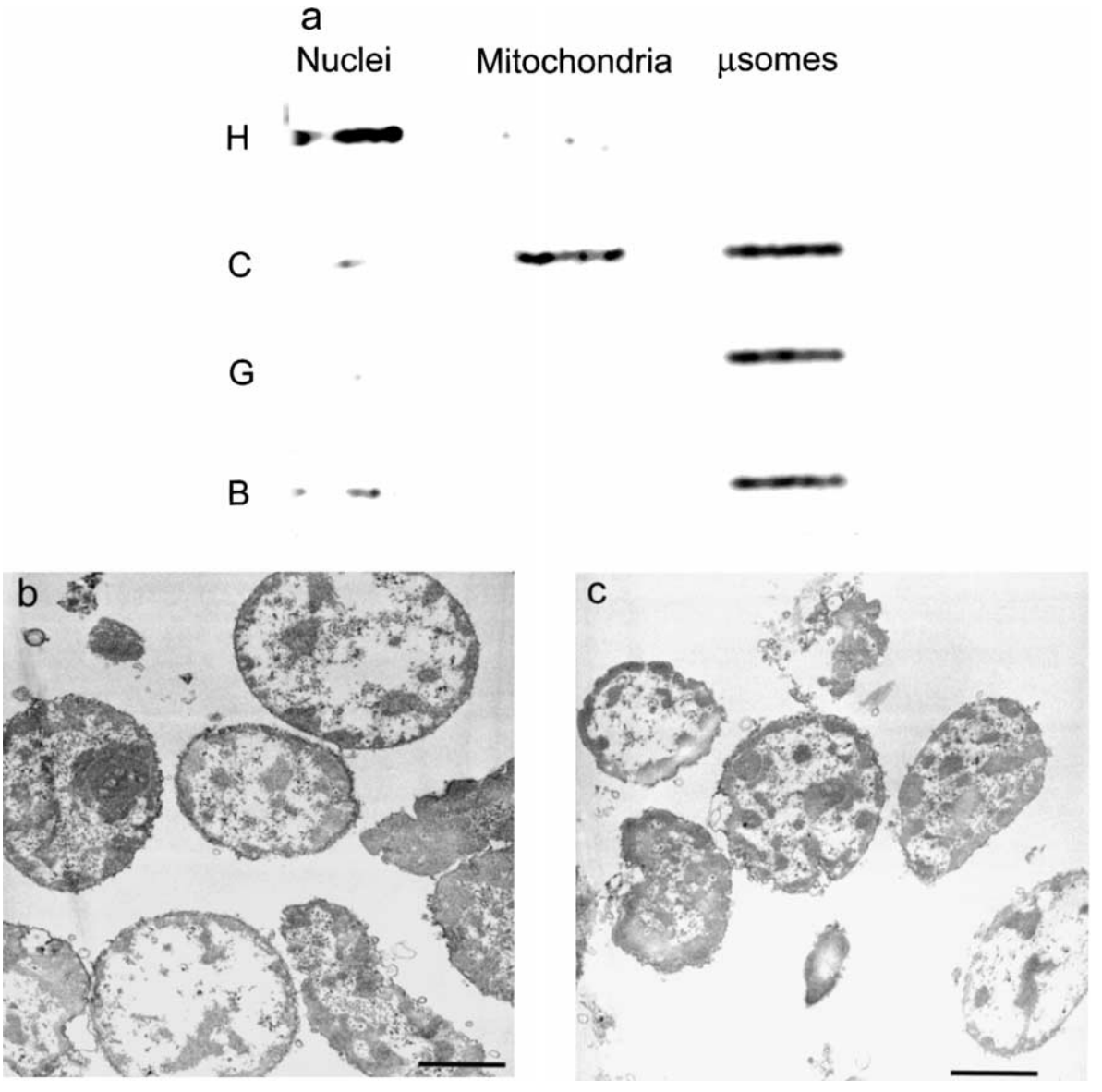

Fig. 1. Evaluation of nuclear fraction purity. (*a*) Representative slot-blot for assessment of purity of isolated rat liver nuclei. The results for the whitish-grey pellet (*nuclei*) and the brown pellet (*mitochondria*) are compared to the results for the microsomal fraction (*μsomes*). Each slot was loaded with 60 μg of the appropriate membrane fraction and probed with antisera to histone (*H*), cytochrome oxidase (*C*), golgi 58K (*G*) or Bip (*B*). (*b*) and (*c*) Representative electron micrographs of the isolated liver nuclei. Bar represents 1 μm.

Birmingham, AL) and coverslips. Fluorescent nuclei were detected using a Nikon Diaphot light microscope (10 × objective) and counted. The A_{260} was determined on equivalent aliquots of unstained nuclei. From these experiments, the following standard curve was obtained: $A_{260} = 0.0058 + 4.85 \times 10^{-8}$ (*N*), where *N* represents the number of nuclei. The number of nuclei in all subsequent experiments was determined from the A_{260} using this relationship.

Nuclear Envelope Isolation

Nuclear envelopes were isolated from rat liver nuclei using a previously published protocol (Dwyer & Blobel, 1976). Briefly, 6×10^9 nuclei (282 A_{260}) were suspended in 3 ml of 10% sucrose in 20 mM triethylamine buffer (TEA buffer) that contained (mM) 0.1 $MgCl_2$, 1 DTT, 0.1 PMSF. The suspension was digested with 600 U of deoxyribonuclease I (DNAase I) and 1 U of ribonuclease A (RNAase A) for 15 min at ambient temperature. After the digestion, the suspension was underlayed with 3 ml of 30% sucrose in TEA buffer and centrifuged at 16,000 × g for 20 min at 4°C. The resulting pellet was resuspended in 3 ml of 10% sucrose in TEA buffer, re-digested, and re-sedimented as described above. The resulting pellet (4.5 mg of protein) was suspended in 250 μl of nuclear storage buffer before storage at −80°C.

Antibody Purification

Antibodies chosen for immunocytochemistry and immunoblot analyses included: 1) a polyclonal anti-peptide antibody, αpan, which recognizes the C-terminus of all three common catalytic subunit isoforms (Garner & Horwitz, 1994); 2) a monoclonal an-

Table 1. 5′-Nucleotidase and Na,K-ATPase activities in rat liver subfractions

Fraction	Protein mg/g_{tissue}	5′-Nucleotidase mmole mg^{-1} min^{-1}	Na,K-ATPase μmole mg^{-1} hr^{-1}
Homogenate	26 ± 4	2.6 ± 0.1	3.8 ± 0.3
Microsomes	7 ± 1	4.0 ± 0.05	8.2 ± 0.1
Nuclei	0.065 ± 0.005	0.5 ± 0.1	6.8 ± 0.2

Mean ± SD for four preparations.

tibody specific for the α1 catalytic subunit isoform (McDonough et al., 1996); 3) polyclonal anti-peptide antibodies specific for the N-terminal (intracellular) region of the α1, α2 and α3 catalytic subunit isoforms (α1IC, α2IC, and α3IC, respectively) (Garner & Kong, 1999); 4) polyclonal anti-peptide antibodies specific for the extracellular region between membrane-spanning sequences 1 and 2 (α1EC, α2EC, and α3EC) (Garner & Kong, 1999); and 5) the polyclonal antibodies (α1FP, α2FP and α3FP) (Shyjan & Levenson, 1989) directed against fusion proteins (FP) containing approximately 180–184 residues of the catalytic domain for the three isoforms. The polyclonal anti-peptide antisera were affinity-purified on Affigel-HZ supports (Bio-Rad) to which the corresponding peptides were attached covalently through a glutaraldehyde linkage (Garner & Kong, 1999). Affinity resin (2 ml, packed) was rinsed with 20 mM Tris buffer (TBST), pH 7.5, containing 150 mM NaCl and 0.15% Tween 20 and mixed with antiserum (0.5 ml diluted with 1.5 ml of TBST) on a shaker for 2 hours at ambient temperature. The resin and bound protein were sedimented by centrifugation (1000 × g, 5 min). The TBST supernatant (preabsorbed antiserum) was saved for use as one of the negative controls. The resin was rinsed with 20 ml of TBST, collected by centrifugation (1000 × g, 2 min), and incubated for 1 min with 2 ml of 0.1 M glycine buffer, pH 2.8. The glycine eluent, containing the eluted antibody, was separated from the affinity resin by centrifugation and immediately neutralized with 82 μl of a 1 M Tris-HCl buffer (pH 9.5). After adding sufficient bovine serum albumin to make a 1% solution, the affinity-purified antibody was dialyzed (100 volumes of TBST containing 0.1 mM NaN_3) before storage at −70°C. The preabsorbed antisera, preimmune sera, normal rabbit serum and α1FP, α2FP and α3FP were affinity-purified on a protein A/G affinity resin (Shah, Tugendreich & Forbes, 1998). Monoclonal pan-anti-histone and anti-splicing factor antibodies and the monoclonal antibody to the Na,K-ATPase α1 isoform were purified by the suppliers.

Immunoblot Analysis

Western blots of SDS-PAGE separations of microsomal fractions from rat brain, rat heart, and rat kidney as well as rat liver nuclei were prepared and stained using previously described methods (Garner & Kong, 1999).

Immunoprecipitation

For immunoprecipitation of renal microsomal Na,K-ATPase, 1 ml of microsomes (3.4 mg/ml in IP buffer: 50 mM Tris-HCl, pH 7.3, containing 150 mM NaCl, 0.5% nonidet P-40 (NP-40), 0.1 mM phenylmethylsulfonyl fluoride, 1 μg/ml leupeptin and 1 μg/ml aprotinin) was precleared by incubation for 90 min with 50 μl of a 50% (v/v) slurry of Protein A-Sepharose (Pharmacia). For immunoprecipitation of Na,K-ATPase from liver nuclei, 4×10^7 nuclei in 500 μl of storage buffer that contained 2% Triton X-100 were incubated for 5 min at 4°C, vortexed for 5 min at room temperature and centrifuged at 15,000 × g for 8 min. The supernatant (nuclear protein fraction) was diluted 1 : 1 with storage buffer to yield a final detergent concentration of 1% and precleared as described previously for the renal microsomes. After removal of the Protein A-Sepharose by centrifugation (2000 × g, 30 sec), 1 μg of affinity-purified polyclonal antibody and 20 μl of a 50% slurry of Protein A-Sepharose were added to the precleared nuclear and renal microsome preparations. These mixtures, after overnight incubation at 4°C on a shaker, were centrifuged at 2600 × g for 30 sec. The supernatant was discarded. The pellet (immunoprecipitate) was rinsed 4 times by resuspension in and recentrifugation from IP buffer. Bound proteins were eluted in 30 μl of SDS-PAGE loading buffer containing 2 μl of β-mercaptoethanol and characterized by SDS-PAGE and immunoblot analysis. For negative controls, the IgG fraction from the preimmune serum replaced the purified polyclonal antibody.

Immunofluorescence microscopy

HepG2 cells on coverslips and rat liver nuclei on polylysine-coated slides were fixed for 10 min with 4% paraformaldehyde in the appropriate buffer (phosphate buffered saline for cells and storage buffer for nuclei), permeabilized with 0.1% Triton X-100 in the appropriate buffer, and finally blocked with 0.5% milk in the appropriate buffer containing 1% normal goat serum. The cells and nuclei were incubated with the affinity-purified anti-peptide antibody (1 : 100 dilution), rinsed with the appropriate buffer and incubated with Alexa-green-labeled goat anti-rabbit IgG (10 μg/ml). A Nikon Diaphot light microscope (40 × objective) was used to visualize the staining. Images were recorded as photomicrographs (exposure times of 10 and 30 seconds for antiserum and negative controls, respectively) that were also used to estimate cellular and nuclear volumes.

Immunoelectron Microscopy

Slices of rat liver, 3 mm thick, were fixed in 4% paraformaldehyde/0.1% glutaraldehyde and embedded in Lowicryl K4M (Polysciences). Thin sections, 0.1 μm, on grids were blocked and permeabilized for five minutes with Tris-buffered saline, pH 7.4, containing 0.05% Triton X-100 and bovine serum albumin (5 mg/ml). The grids were incubated for 4 hours with the primary antibodies or preabsorbed antibodies, rinsed and incubated for one hour with goat anti-rabbit IgG coupled to 15-nm or 20-nm gold particles. After rinsing to remove the secondary antibody, the sections were post-fixed (2% glutaraldehyde) and stained with uranyl acetate and lead citrate (Garner & Kong, 1999). The sections were studied with a Zeiss 910 transmission microscope. The total area studied and documented with photographs was 20 μm^2 for the preabsorbed antisera (negative controls), 40 μm^2 for the pan-catalytic subunit antiserum, and 20 μm^2 for each of the polyclonal antisera to the α1, α2 and α3 catalytic subunits. To determine the gold-particle counts in the nuclear envelope (outer and inner membranes), nucleoplasm and non-nuclear compartments, negatives were scanned (Umax PowerLook II) at 600dpi in RGB mode with the auto-adjust on. Each scanned image was opened in Adobe Photoshop 5.0 (Adobe Systems), inverted and the levels adjusted. The threshold was adjusted until all non-gold material was eliminated. The image was converted to greyscale before being transferred to NIH Image™ for particle counting. Instat 2.03 and Statview 4.02 programs were used to search for significant differences in staining. While all distributions were normal, there were significant differences among the standard deviations of the means. Therefore the Mann-Whitney test, which compares the medians of two unpaired populations, was employed instead of the unpaired Student's *t*-test to identify significant differences in the counts.

$^{22}Na^+$ and $^{86}Rb^+$ Influx Experiments with Isolated Liver Nuclei

The influx of $^{22}Na^+$ and $^{86}Rb^+$ into isolated nuclei was determined in transport medium (in mM: 25 HEPES, 135 KCl, 2 K_2HPO_4, 10 NaCl, 4 $MgCl_2$, 1 DTT, 3 ATP [Tris salt], and 1% dimethylsulfoxide; pH was adjusted to 7.2 with 2 M KOH) in the presence or absence of 0.1 mM ouabain. Since one of the rat Na,K-ATPase catalytic subunit isoforms has a very low affinity for cardiac glycosides, ouabain was used for these experiments with isolated rat liver nuclei instead of the more membrane-permeable, but less water-soluble aglycone, K-strophanthidin. In a typical experiment, nuclei (3×10^7) were suspended in 1.3 ml of the appropriate transport medium and incubated at 37°C for 30 min before $^{22}Na^+$ (1 μCi/ml) or $^{86}Rb^+$ (2 μCi/ml) was added. At selected time intervals, over a two-hour period after the addition of isotope, 250-μl aliquots were withdrawn: (i) 10 μl of each aliquot were placed in vials with 10 ml of scintillation fluid and counted (cpm_{med}); (ii) nuclei from 150 μl were collected on nitrocellulose filters, rinsed with 10 ml of the appropriate label-free transport medium, placed in vials with 10 ml of scintillation fluid and counted (cpm_{filter}); (iii) 50 μl of each 250-μl aliquot were diluted 1:10 with ATP-free transport medium and centrifuged (12,500 × g, 2 min). After the resultant pellet had been rinsed three times with ATP-free transport medium, the A_{260} was measured to determine the exact number of nuclei in each 250-μl aliquot. Plots of the cpm_{filter}/cpm_{med} ratio versus time were fit to a first-order rate expression, $cpm_{filter}/cpm_{med} = (cpm_{filter}/cpm_{med})_{max}(1 - e^{-kt})$, where k is the first-order rate constant and $(cpm_{filter}/cpm_{med})_{max}$ is the limiting ratio as $t \to \infty$. R^2 values ≥ 0.97 were obtained for all fits. The $(cpm_{filter}/cpm_{med})_{max}$ values and a nuclear volume of 92 fl (*see* above) were used to determine the ratio, cpm per ml nuclei: cpm per ml medium. These ratios and the known concentrations of Na^+ and K^+ in the medium were used to calculate steady-state nuclear Na^+ and K^+ levels.

$^{86}Rb^+$ Influx into Cytoplasm and Nuclei of HepG2 Cells

The influx of $^{86}Rb^+$ into HepG2 cells was studied using a modification of a procedure described previously for the cultured lens epithelium (Garner et al., 1992). HepG2 cells (10^6 to 10^7 cells, harvested and plated in individual wells of 6-well plates 15 hr prior to the experiment) were incubated in minimal essential medium (MEM Eagles) containing 10% fetal bovine serum and 1 μCi/ml $^{86}Rb^+$ with or without K-strophanthidin (0.1 mM nominal concentration; actual concentration ≤0.1 mM, based on the octanol/water partition coefficient (Dzimiri, Fricke & Klaus, 1987)). While K-strophanthidin is more membrane-permeable than ouabain, it is two orders of magnitude less potent (Dzimiri et al., 1987). The potency and water-insolubility do not present a problem for the human Na,K-ATPases of the HepG2 cells since all isoforms have relatively high affinities for cardiac glycosides and their aglycones (Crambert et al., 2000). Both media (i.e., with and without K-strophanthidin) contained 1% DMSO, the solvent required for the strophanthidin stock solution. At predetermined times over a three-hour period, medium was removed from selected cultures and the cells were rinsed five times with phosphate buffered saline. The cells were harvested by scraping in 2 ml of storage buffer and sedimented by centrifugation. After removal of the supernatant, the sedimented cells were disrupted in 1 ml of storage buffer (5 strokes in a 1-ml Duall tissue grinder), mixed with 1 ml of 1.6 M sucrose and centrifuged at 19,000 × g for 15 min at room temperature. The supernatant was removed, placed in a vial with scintillation fluid and counted (cpm_{sup}). The pellet, containing nuclei, was rinsed 3 times with storage buffer and treated with 0.1 M NaOH (1 hr, 60°C). After centrifugation (19,000 × g, 15 min) the NaOH supernatants were placed in vials with scintillation fluid and counted (cpm_{NaOH}). Plots of cpm_{sup} (cytoplasmic) and cpm_{NaOH} (nuclear) versus time were fit to the first-order expression $cpm = cpm_{max}(1 - e^{-kt})$. Cellular and nuclear volumes (mean ± SD, n = 30), estimated from light and electron micrographs (as described above for isolated nuclei) were 1.1 ± 0.3 (10^{-8}) ml and 8.9 ± 3.0 (10^{-11}) ml, respectively. Cpm_{max} values from the cytoplasmic and nuclear fits, along with cell and nuclear volumes, were used to calculate cpm/ml cytoplasm : cpm/ml incubation medium ($cpm_{cytoplasm}/cpm_{medium}$) and cpm/ml nucleus : cpm/ml cytoplasm ($cpm_{nucleus}/cpm_{cytoplasm}$). These ratios and the K^+ concentration in the incubation medium were used to calculate steady-state K^+ levels in the cytoplasmic and nuclear compartments.

Determination of Nucleoplasmic and Lumenal Na^+ and K^+ Concentrations

Sodium-green dextran, a single-wavelength indicator, and Texas-red dextran, a cation-independent fluorescent dye, were used for the ratiometric determination of nucleoplasmic Na^+ concentrations. Isolated rat liver nuclei (10^9 nuclei) were gently mixed at 37°C, in the dark, for 60 min, with 0.004 μM Texas-red dextran and 0.020 μM sodium-green dextran in FLUOR buffer. FLUOR buffer was composed of (in mM) 25 HEPES (free acid), 2 Tris phosphate (dibasic salt), 3 ATP (Tris salt), 5 $MgCl_2$, 1 DTT, 140 KCl, 10 NaCl and sufficient Tris base to obtain a pH of 7.3. The free indicators were separated from the nuclei by sedimentation (3000 × g, 2 min). The supernatant was removed and saved; the pellet was rinsed 5 to 8 times with FLUOR buffer to remove all unloaded dye and resuspended in FLUOR buffer to a concentration of 10^9 nuclei/ml. Thirty-microliter aliquots of the suspension were transferred to quartz cuvettes that contained 3 ml of one of the following solutions: 1) FLUOR buffer; 2) FLUOR buffer containing 0.1 mM ouabain; 3) FLUOR buffer that contained 0.1% Triton X-100; or 4) FLUOR buffer that contained 0.1 mM ouabain and 0.1% Triton X-100. (Note: Triton X-100 was used for these experiments because NP-40 interfered with the Texas-red fluorescence). Emission spectra were determined at 37°C by synchronous scan with a 30-nm separation between excitation and emission wavelengths using an Aminco Bowman Series 2 Luminescence Spectrometer fitted with a thermostated stirred cell holder. The fluorescence intensity of sodium-green dextran at 535 nm (F_{SGDX}), Texas-red-dextran at 616 nm (F_{TRDX}) and the ratio F_{SGDX}/F_{TRDX} were determined from the spectra.

SBFI and PBFI were used for the ratiometric determination of lumenal Na^+ and K^+ concentrations, respectively. Nuclei (10^9 nuclei/ml) were suspended in FLUOR buffer that contained 0.5 mM SBFI-am or 0.5 mM PBFI-am and pluronic acid. After a 60-min incubation at 4°C, in the dark with mixing, the excess indicator was removed by centrifugation (as described previously for the dextrans) and the nuclear pellet was rinsed 5–8 times by resuspension in and recentrifugation from FLUOR buffer. The time trace of the ratio of the luminescence intensity at 505 nm following excitation at 340 and 380 nm was obtained at 37°C in the stirred cell, using the dual-excitation intracellular-acquisition program for the Aminco Bowman luminescence spectrometer. At selected times, ouabain and/or NP-40 (final concentrations of 0.1 mM and 0.1%, respectively) were added by syringe pump during the measurement.

For the experiments with sodium-green dextran, standard curves were prepared by titrating the sodium-green dextran/Texas-red dextran mixture with Na^+ under conditions of constant ionic strength, with $[Na^+] + [K^+] = 150$ mM. For experiments with SBFI and PBFI, standard curves were prepared by measuring the F_{340}/F_{380} ratio of 1 μM SBFI or PBFI in FLUOR buffer with varying concentrations of Na^+ and K^+ at fixed ionic strength, where $[Na^+] + [K^+] = 150$ mM. To obtain the standard curves, the data were fit to the following equation:

Table 2. Nuclear Na^+ and K^+ concentrations measured by radioisotope influx

Isotope	Sample	Inhibitor	Ion concentration (mM)	Ratio (cpm/cpm)	Ion concentration (mM)
$^{22}Na^+$	Nuclei	−Ouabain	$[Na^+]_{med}$: 10	Nuc/med: 1.0 ± 0.2 (10)	$[Na^+]_{nuc}$: 10 ± 1
		+Ouabain	10	0.5 ± 0.2 (10)*	5 ± 1*
$^{86}Rb^+$	Nuclei	−Ouabain	$[K^+]_{med}$: 139	Nuc/med: 0.99 ± 0.22 (4)	$[K^+]_{nuc}$: 138 ± 23
		+Ouabain	139	1.19 ± 0.08 (4)*	165 ± 10*
$^{86}Rb^+$	Cells	−Strophantidin	$[K^+]_{med}$: 5	Cyt/med: 22.1 ± 7.6 (4)	$[K^+]_{cyt}$: 111 ± 38
		+Strophantidin	: 5	1.4 ± 0.4 (4)*	: 7 ± 2*
$^{86}Rb^+$	Cells	−Strophantidin	$[K^+]_{cyt}$: 111 ± 38	Nuc/cyt: 0.9 ± 0.2	$[K^+]_{nuc}$: 99 ± 25
		+Strophantidin	: 7 ± 2*	3.2 ± 0.3*	23 ± 2*

*Indicates a statistically significant difference between values in the absence and presence of ouabain (unpaired t-test, $p \leq 0.057$). Cyt, cytoplasm; med, culture medium; nuc, nucleus.

$$F = F_i + \{(F_f - F_i)/(1 + K_{M^+}/[M^+])\}$$

F is the observed fluorescence intensity (e.g., F_{SGDX}) or ratio of fluorescence intensities (e.g., F_{SGDX}/F_{TRDX}). F_i and F_f are the fluorescence intensities or ratio of fluorescence intensities as $[M^+]$ (Na^+ or K^+) approaches limiting values of 0 and ∞, respectively. K_{M^+} is the concentration of M^+ at 50% of the total change in fluorescence intensity or fluorescence intensity ratio.

The standard curves for F_{SGDX}/F_{TRDX} and F_{340}/F_{380} and the ratios of the fluorescence intensities for the dye-loaded nuclei were used to determine the steady-state nucleoplasmic Na^+ and lumenal Na^+ and K^+ concentrations, respectively.

Curve fitting was performed using three programs, each with a unique fitting algorithm [Kaleidagraph™, 3.0.4 (Abelbeck Software), SigmaPlot, 4.17 (Jandel Scientific) and MacCurveFit, 1.5.2 (Kevin Raner Software)]. For each data set, all three programs yielded the same constants and R^2 values. Figures in this report were prepared using Kaleidagraph™.

Results

Na^+ and K^+ concentrations in the nucleus

Steady-state Na^+ and K^+ concentrations ($[Na^+]_{nuc}$ and $[K^+]_{nuc}$, respectively, Table 2) were determined in isolated rat liver nuclei (Fig. 1), using $^{22}Na^+$ and $^{86}Rb^+$ as tracers for Na^+ and K^+, respectively, in the presence and absence of ouabain, a prototypical cardiac glycoside, which inhibits Na^+ and K^+ transport across the plasma membrane by inhibiting Na,K-ATPase (Noel, Fagoo & Godfraind, 1990). In the presence of ouabain, there was a statistically significant decrease ($p < 0.01$) in the $cpm_{nucleus}/cpm_{medium}$ ratio for $^{22}Na^+$, which translated into an ~50% decrease in the nuclear Na^+ concentration, and an apparent increase (ns, $p = 0.057$) in the $cpm_{nucleus}/cpm_{medium}$ ratio for $^{86}Rb^+$, which suggested a potential 20% increase in the nuclear K^+ concentration. In the absence of the cardiac glycoside, there was no apparent difference in Na^+ and K^+ concentrations between nucleus and medium (which represented the cytoplasm in these experiments), since the $cpm_{nucleus}/cpm_{medium}$ ratios were approximately 1.

Experiments were performed to determine whether the results with isolated nuclei were representative of nuclei in intact cells. Steady-state K^+ concentrations, using $^{86}Rb^+$ as a tracer for K^+, were estimated in the nuclei of HepG2 cells that were incubated in culture medium in the presence or absence of a Na,K-ATPase inhibitor. In these experiments, K-strophanthidin (the membrane-permeable aglycone of K-strophanthin) was used instead of ouabain (*see* Materials and Methods for additional details). Based on the well understood effects of cardiac glycosides and their aglycones on Na,K-ATPase function, K-strophanthidin should cause a dissipation of the trans-plasma membrane K^+ gradient. Indeed, this effect was observed in the HepG2 cells. The $cpm_{cytoplasm}/cpm_{medium}$ ratio for $^{86}Rb^+$ approached 1.0 in the presence of K-strophanthidin, demonstrating that, with inhibition of plasma membrane Na,K-ATPases, the cytoplasmic K^+ levels approximated that of the extracellular medium (Table 2). In these same cells, K-strophanthidin, introduced to the extracellular compartment, caused a statistically significant increase in the $cpm_{nucleus}/cpm_{cytoplasm}$ ratio from 0.9 to 3.2 (Table 2).

In both the experiments with isolated nuclei and the experiments with HepG2 cells, a Na,K-ATPase inhibitor unmasked gradients between the extranuclear compartment and the nucleus. One way to explain these transport results is to propose that the Na,K-ATPase inhibitors dissipated a gradient across the fluid compartment that separates cytoplasm and nucleoplasm, i.e, the nuclear envelope lumen. In this model, the Na^+ and K^+ concentrations of the intact nucleus (nucleoplasm + nuclear envelope lumen) observed in the presence of the Na,K-ATPase inhibitors would approximate the Na^+ and K^+ concentrations of the nucleoplasm, since the nucleoplasm represents 94% of the total nuclear volume. The lumenal Na^+concentration would have to be sufficiently high and the lumenal K^+ concentration sufficiently low to yield the observed concentrations in the intact nucleus in the absence of inhibitors (Table 2). To test this hypothesis, the nucleoplasmic and

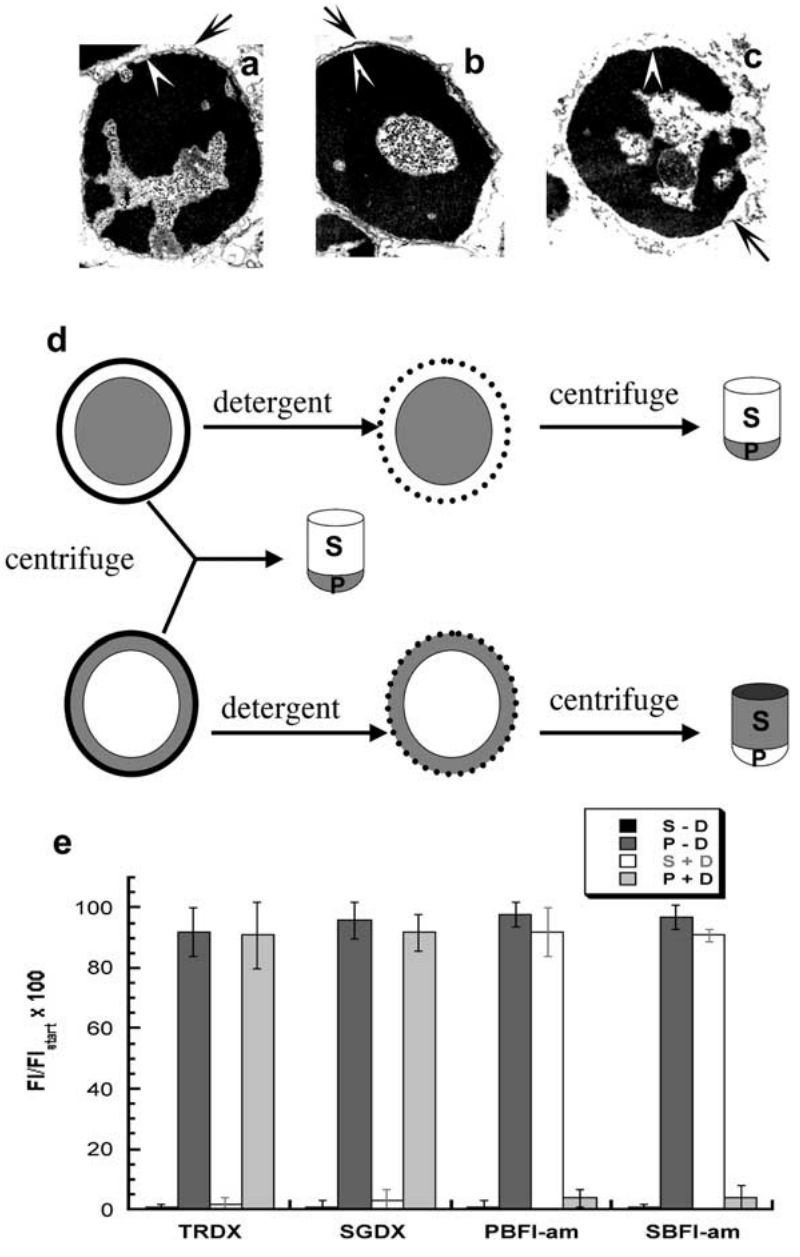

Fig. 2. Differential detection of Na^+- and K^+-dependent fluorescence in the nucleoplasm and nuclear envelope lumen. Representative electron micrographs showing selective removal of the outer nuclear membrane: (*a*) freshly prepared rat liver nuclei, (*b*) nuclei loaded with Texas-red dextran, and (*c*) nuclei loaded with Texas-red dextran and treated with 0.1% Triton X-100. Black arrows indicate the outer membrane of the nuclear envelope; white arrowheads, the inner membrane. (*d*) Schematic depicting the experimental approach to differentiate between nucleoplasmic and lumenal fluorescent dye localization (*S*, supernatant; *P*, pellet). (*e*) Localization of fluorescence in nuclei loaded with Texas-red dextran (TRDX), sodium-green dextran (SGDX), PBFI-am or SBFI-am in the presence (+) or absence (−) of detergent (*D*). The results relative to the fluorescence intensity prior to fractionation (FI_{start}) are plotted as mean ± standard deviation of quadruplicate determinations.

lumenal monovalent cation concentrations were estimated using cation-selective indicators.

Nuclear Location of TRDX, SGDX, PBFI and SBFI

As demonstrated in a previous study of nuclear Ca^{2+} homeostasis (Gerasimenko et al., 1995), fluorescent indicator dextrans enter the nucleoplasm of isolated nuclei via the nuclear pore. In contrast, nonfluorescent, membrane-permeable acetoxymethyl (am) indicators enter the nuclear envelope lumen and are hydrolyzed to membrane-impermeable fluorescent indicators by resident esterases, thereby trapping them in the nuclear envelope lumen (Gerasimenko et al., 1995). Therefore, by analogy with the aforementioned study using Ca^{2+} indicators, the sodium-sensitive indicator, SBFI-am, and the potassium-sensitive indicator, PBFI-am, should be useful for determination of lumenal Na^+ and K^+ concentrations. The sodium-sensitive indicator, sodium-green dextran (SGDX), should be useful for determination of nucleoplasmic Na^+ concentrations. A dextran derivative of a potassium-sensitive indicator is currently unavailable for use in measuring nucleoplasmic K^+ concentrations.

The most direct method for visualizing the location of the fluorescent indicators is multiphoton confocal microscopy as was used in the previous study with Ca^{2+} indicators (Gerasimenko et al.,

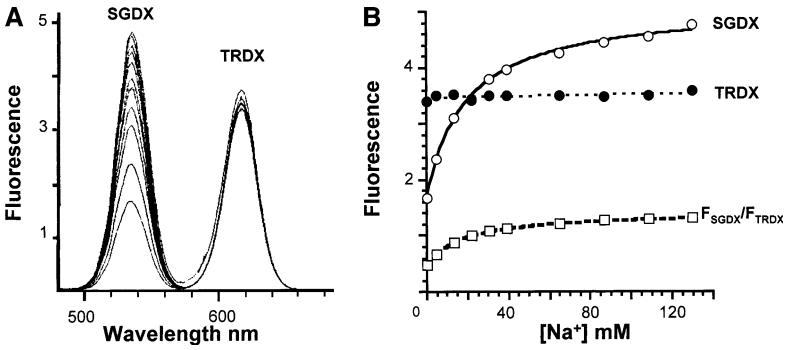

Fig. 3. Standard curve for the TRDX-SGDX couple. (*a*) Representative emission spectra for the titration of the TRDX-SGDX couple with Na^+ (0–150 mM) at constant ionic strength with ($[Na^+]$ + $[K^+]$ = 150 mM. Final concentrations of the TRDX and SGDX were 0.1 pmol/ml and 0.5 pmol/ml, respectively. (*b*) Plots of the fluorescence intensity of the SGDX (*empty circles*), TRDX (*filled circles*) and the ratio of the fluorescence intensities of the two indicators (F_{SGDX}/F_{TRDX}, empty squares) versus the Na^+ concentration.

Table 3. Nucleoplasmic sodium concentrations

Sample	F_{SGDX}/F_{TRDX}†	$[Na^+]_{NPL}$†*
Nuclei	0.59 ± 0.05	2.1 ± 1.13
Nuclei + detergent	0.62 ± 0.03	2.9 ± 0.08
Nuclei + ouabain	0.66 ± 0.04[a]	4.0 ± 1.1
Nuclei + detergent + ouabain	0.79 ± 0.04[a,b,c]	8.5 ± 1.6

†Results are reported as mean ± SD for quadruplicate determinations for two preparations of nuclei.
[a]Value is significantly different from Nuclei, $p < 0.02$, student t test.
[b]Value is significantly different from Nuclei + detergent, $p < 0.0001$.
[c]Value is significantly different from Nuclei + ouabain, $p < 0.0001$.
*$[Na^+]_{NPL}$ determined from F_{SGDX}/F_{TRDX} values and standard curve of F_{SGDX}/F_{TRDX} *vs.* $[Na^+]$ (Fig. 3*b*)

1995). For the present study, a confocal microscope appropriately configured for the Na^+, K^+ and Texas-red indicators was unavailable. Since the main objective was the quantitation of steady-state lumenal and nucleoplasmic Na^+ and K^+ levels, a method was developed that took advantage of the stirred cell and fluorometer currently in the laboratory. A differential method, based on selective removal of the outer nuclear membrane (Fig. 2*a-c*), was developed to distinguish between, as well as to quantify, lumenal and nucleoplasmic fluorescence (Fig. 2*d*). The outer membrane of the nuclear envelope can be selectively disrupted with 0.1% (v/v) Triton X-100 (Neitcheva & Peeva, 1995), as demonstrated in the electron micrographs of Fig. 2*a-c*. Nuclei (panel *a*) were loaded with dye (panel *b*) and treated with detergent (panel *c*). The dilute detergent disrupted only the outer membrane of the nuclear envelope; the inner membrane of the nuclear envelope remained intact (panel *c*). This means that nucleoplasmic fluorescence should remain with the sedimented nuclei (the pellet, *P*, after centrifugation) in the absence or presence of detergent (Fig. 2*d*). The lumenal fluorescence should remain with fraction *P* in the absence of detergent but should be found in the supernatant (*S*) fraction in the presence of detergent. To validate this experimental approach, the fluorescence spectra were determined for nuclei loaded with the indicators. Then, the indicator-loaded nuclei were incubated for five minutes in the presence or absence of 0.1% detergent and the *S* and *P* fractions isolated by centrifugation. The isolated nuclei (*P*) were resuspended and the fluorescence spectra of the two fractions (*S* and *P*) were redetermined. The results of these experiments (Fig. 2*e*) show that the SBFI and PBFI were released into the supernatant (*S*) by detergent treatment. Conversely, the sodium-green dextran (SGDX) and the Texas-red dextran (TRDX) remained with the nuclei (*P*) after detergent treatment. In other words, the SBFI and PBFI were localized in the nuclear envelope lumen and the two indicator-dextrans were localized in the nucleoplasm, exactly as expected. The results with the SBFI-am and PBFI-am also confirmed the previous report of lumenal esterase activity (Gerasimenko et al., 1995).

Na^+ Concentrations in the Nucleoplasm

Since sodium-green dextran is a single-wavelength Na^+ indicator, the cation-independent indicator, Texas-red dextran, was used to correct for inter-sample differences in absolute indicator concentration. First, standard curves were prepared. A mixture of the two fluorescent dextrans as titrated with Na^+ under conditions of constant ionic strength, with $[Na^+]$ + $[K^+]$ = 150 mM. Emission spectra are displayed in Fig. 3*a*, for a representative data set. While the fluorescence intensity of the sodium-green dextran increased with increasing $[Na^+]$ (Fig. 3*a*, 535 nm; Fig. 3*b*, F_{SGDX}), the fluorescence intensity of Texas-red dextran was relatively constant (Fig. 3*a*, 616 nm; Fig. 3*b*, F_{TRDX}). Values for F_i, F_f and K_{Na} (*see* Methods for a definition of these terms) were 1.71 ± 0.05, 5.12 ± 0.06, and 19.7 ± 1.48 mM, respectively, for the fit to the F_{SGDX} data (R^2 = 0.998). Values of F_i, F_f and K_{Na} were 0.492 ± 0.005, 1.44 ± 0.006 and 18.5 ± 0.5 mM, respectively, for the fit to the F_{SGDX}/F_{TRDX} data (R^2 = 1.0). The K_{Na} values reported here (19.7 and 18.5 mM) are comparable to the previously reported value for sodium-green dextran (21 mM), titrated with Na^+ at a slightly lower constant ionic

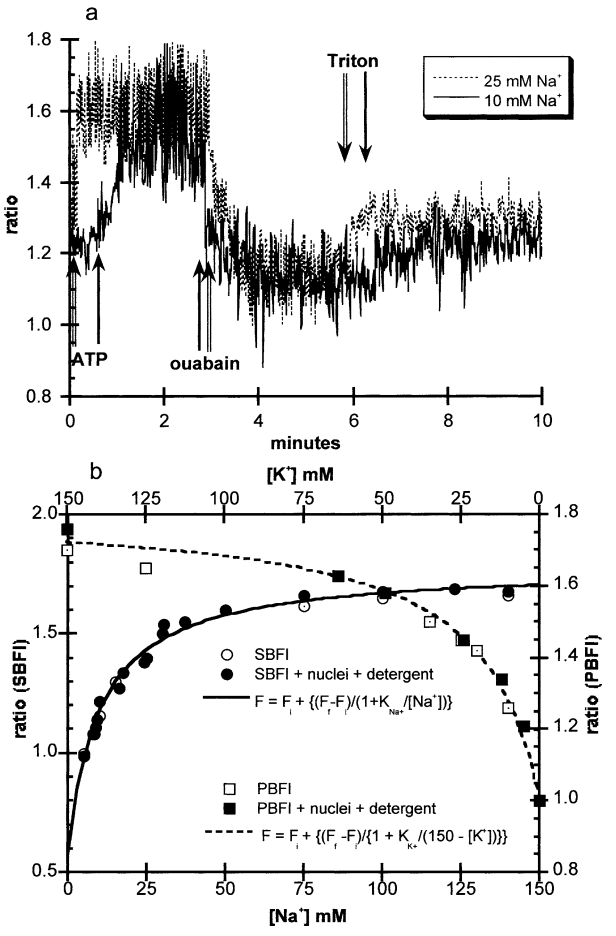

Fig. 4. Results with SBFI and PBFI for lumenal Na^+ and K^+.(*a*) Traces for SBFI-loaded nuclei suspended in FLUOR buffer containing 10 mM Na^+ + 140 mM K^+ (*solid line*, *solid arrows*) or in FLUOR buffer containing 25 mM Na^+ and 125 mM K^+ (*dotted line*, *double-lined arrows*). In both instances the suspended nuclei were treated sequentially with ATP (*left arrows*; final [ATP] = 3 mM), ouabain (*center arrows*; final [ouabain] = 0.1 mM), and Triton X-100 (*right arrows*; final Triton X-100 concentration = 0.1% v/v). (*b*) Titration of SBFI with Na^+ (*empty circles*) and PBFI with K^+ (*empty squares*) at constant ionic strength ([Na^+] (*lower X axis*) + [K^+] (*upper X axis*) = 150 mM). Values for K_{Na^+} for SBFI and K_{K^+} for PBFI were 10.1 ± 1.6 mM and 19.4 ± 2.1 mM, respectively. Ratio of SBFI-loaded nuclei (*filled circles*) and PBFI-loaded nuclei (*filled squares*) after treatment with Triton X-100. The error bars (± SD, n = 4 experiments) fall inside the data points used in the figure.

strength, where [Na^+] + [K^+] = 135 mM (Szmacinski & Lakowicz, 1997).

In the next set of experiments, the F_{SGDX}/F_{TRDX} ratio (i.e., normalized Na^+-dependent fluorescence) was determined for freshly prepared rat liver nuclei in the absence or presence of ouabain and/or detergent (Table 3). For consistency with the studies described in Table 2, the experiments were performed at an extranuclear sodium concentration of 10 mM. There was a significant increase in the normalized Na^+-dependent fluorescence in the presence of ouabain, a result consistent with ouabain's role as a Na,K-ATPase inhibitor (Lingrel et al., 1997; Blanco & Mercer, 1998). The observed changes in fluorescence translated into an apparent increase in the nucleoplasmic Na^+ concentration from 2.1 to 4.0 mM in intact nuclei and 2.9 to 8.5 mM in nuclei where the outer membrane of the nuclear envelope was compromised by detergent treatment. In the absence of ouabain, the addition of detergent to compromise the outer membrane of the nuclear envelope had no effect on the F_{SGDX}/F_{TRDX}, hence on the nucleoplasmic Na^+ concentration.

Taken together, these results indicate that Na,K-ATPase is in the inner membrane of the nuclear envelope with the ouabain site in the lumen. First, the Na^+ gradient between the extranuclear compartment and nucleoplasm was maintained even after the integrity of the outer membrane was compromised. Second, ouabain's elevation of nucleoplasmic Na^+ concentration was more pronounced after detergent treatment, suggesting that the ouabain binding site became more accessible, i.e., the ouabain site is lumenal: therefore the catalytic site is nucleoplasmic. This deduced orientation is further substantiated by the immunogold results described later in this report. Finally, since ouabain caused nucleoplasmic Na^+ levels to approach extranuclear Na^+ levels in detergent-treated nuclei but not in intact nuclei, these data strongly indicate that the nuclear envelope is not freely permeable to Na^+. It should be pointed out that reduced extranuclear K^+ levels existed in the HepG2 cells when the plasma membrane Na,K-ATPase was inhibited with K-strophanthidin (Table 2), yet the nuclear K^+ concentration remained higher than the medium, suggesting that the nuclear envelope is not freely permeable to K^+, either.

Na^+ and K^+ Concentrations in the Nuclear Envelope Lumen

Lumenal Na^+ and K^+ concentrations were estimated using dual-wavelength indicators, SBFI for Na^+ and PBFI for K^+. With these indicators, the normalized Na^+- or K^+-dependent fluorescence (F_{340}/F_{380} ratio) increases with increasing Na^+ or K^+ concentration under constant ionic strength conditions (i.e., [Na^+] + [K^+] = 150 mM), Fig. 4*b*. The data for SBFI and PBFI were fit to the equations indicated in Figure 4. The values from these fits were used to calculate Na^+ and K^+ concentrations in subsequent experiments with SBFI- or PBFI-loaded nuclei.

The results with SBFI-loaded nuclei demonstrated an ATP-dependent maintenance of Na^+ levels in the nuclear envelope lumen. For the SBFI-loaded nuclei in the absence of ATP, the F_{340}/F_{380} ratio was constant, 1.19 ± 0.05, with increasing concentrations of extranuclear Na^+ under conditions of constant ionic strength. Fig. 4*a*, shows representative tracings

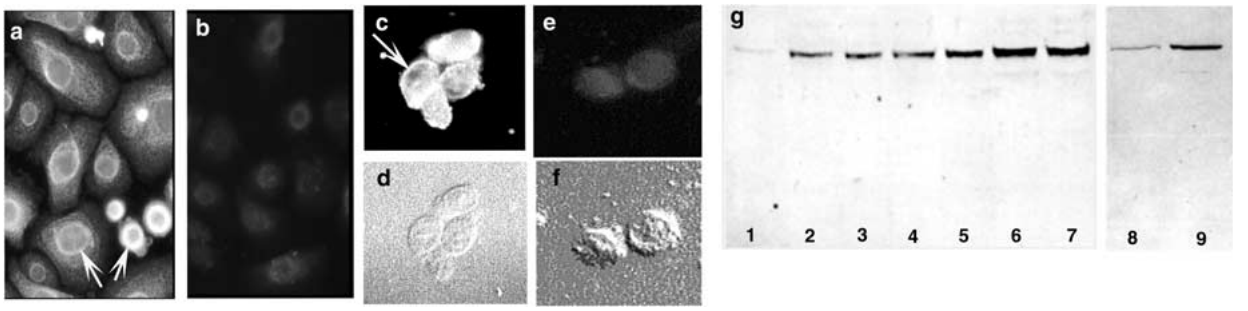

Fig. 5. Immunochemical detection of Na,K-ATPase. (*a–f*) Indirect immunofluorescence. Na,K-ATPase detected in HepG2 cells (*a*) and rat liver nuclei (*c*) using affinity-purified anti-Na,K-ATPase (catalytic subunit). Representative negative controls: (*b*) HepG2 cells treated with the IgG fraction from preimmune serum and (*e*) rat liver nuclei treated with non-immune rabbit IgG. (*d*) and (*f*) are Nomarski images of the same fields as (*c*) and (*e*), respectively. (*g*) Immunoblot studies. Lanes *1–4*, containing 10, 20, 40, and 50 μg, respectively, of rat liver nuclear protein and lanes *5*, *6*, and *7*, containing 50 μg of rat heart, rat brain and rat renal microsomal protein, respectively, stained with affinity-purified anti-Na, K-ATPase (catalytic subunit). Lanes *8* and *9* show the results for the immunoprecipitation of the nuclear and renal microsomal protein fractions, respectively, with affinity-purified anti-Na, K-ATPase (catalytic subunit), followed by immunoblotting and staining with a mouse monoclonal antibody specific for the α1 catalytic subunit isoform.

Table 4. $[Na^+]$ and $[K^+]$ in the Nuclear Envelope Lumen [NEL]

		F_{340}/F_{380} Mean ± SD	Concentration Mean (mM)	Concentration Range (mM) (± 1 SD from the mean)
SBFI-am (n = 10)	Nuclei + ATP	1.65 ± 0.04	$[Na^+]$: 84	$[Na^+]$: 62 – 125
	Nuclei + ATP + ouabain	1.10 ± 0.05	8	7 – 9
PBFI-am (n = 6)	Nuclei + ATP	1.17 ± 0.07	$[K^+]$: 5	$[K^+]$: 2 – 8
	Nuclei + ATP + ouabain	1.52 ± 0.06	32	24 – 45

$[Na^+]$ and $[K^+]$ were determined using the equation for the standard curves (Fig. 4*b*).

for two of the 17 different Na^+ concentrations that were used for SBFI-loaded nuclei. With the addition of ATP, the normalized fluorescence (F_{340}/F_{380} ratio) increased to a higher constant value of 1.65 ± 0.04 (Table 4), corresponding to a lumenal Na^+ concentration of 84 mM. The subsequent addition of ouabain caused the normalized fluorescence intensity to decrease to a constant value (1.10 ± 0.05), which corresponded to a lumenal Na^+ concentration of 8 mM. Finally, the addition of detergent caused the normalized fluorescence intensity to increase or decrease, depending upon the Na^+ concentration of the medium (Fig. 4*b*, *filled circles*). In fact, the data points for the detergent-treated nuclei in media of increasing Na^+ concentrations fall on the standard curve for the titration of SBFI (free dye) with Na^+ (Fig. 4*b, empty circles*).

These results with SBFI unequivocally validate the methodology employed here. First, the data points in the presence of detergent fell on the standard curve that was constructed with free dye. Second, the nuclei were loaded with the nonfluorescent ester derivative of the dye, which had to be cleaved to become a sodium indicator. Third, the signal-to-noise ratios (S/N) indicated the location of the dye. The S/N was 15 ± 7 in stirred suspensions of intact nuclei, where the dye was tumbling with the scatter elements (i.e., the individual nuclei) (*see* Fig. 4*a*, time period prior to Triton addition). The S/N increased to 35 ± 5 in the stirred suspensions of nuclei after the addition of detergent, when the water-soluble indicator was released and tumbling at its own rate in the solution in which the scatter elements were suspended. The S/N increased to 50 ± 8 when the detergent-treated nuclei (scatter elements) were sedimented.

For PBFI-loaded nuclei, the effects of ATP and ouabain on lumenal K^+ levels (F_{340}/F_{380} ratio) were opposite those observed for Na^+ in SBFI-loaded nuclei (Table 4). For extranuclear $[K^+] \geq 10$ mM, ATP decreased the normalized fluorescence intensity to virtually the same value (1.17 ± 0.07, equivalent to a lumenal K^+ concentration of 5 mM) for all seven K^+ concentrations that were tested. At all extranuclear K^+ concentrations, ouabain caused the normalized fluorescence intensity to increase to a new constant value of 1.52 ± 0.06, which corresponded to roughly a six-fold increase in lumenal K^+ concentration. Lastly, the addition of detergent caused the normalized fluorescence intensity to approach that predicted for the K^+ concentrations of the extranuclear milieus (Fig. 4*b*, *filled squares*). As was the case for the Na^+ indicator, the data points for detergent-treated nuclei in media of increasing K^+ concentrations fall on the standard curve for the titration of

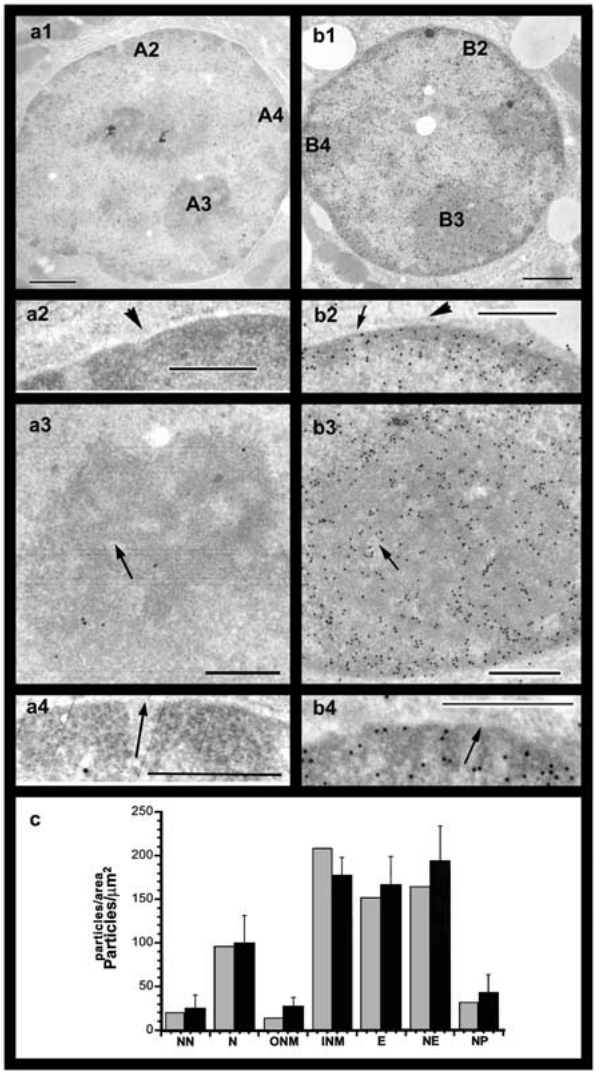

Fig. 6. Detection of Na, K- ATPase by immunogold electron microscopy. (*a1*) Representative control, a liver section stained with the preabsorbed pan-catalytic subunit IgG fraction. (*a2*, *a3*, *a4*) Higher magnification of the nucleus in a1, regions A2, A3, and A4, respectively; arrowheads indicate the outer membrane of the nuclear envelope. (*b1*) Representative micrograph of a liver section stained with affinity-purified, pan-catalytic subunit antibody and gold-labeled-GAR. (*b2*) Higher magnification of region B2 (panel *b1*) where the envelope is cut transversely; arrow indicates a nuclear pore. (*b3*) Higher magnification of region B3 (panel *b1*), a region where the envelope is cut tangentially so that the heterochromatin underlying the nuclear envelope is punctuated with circular, heterochromatin-free pores (60–70 nm in diameter); representative pore indicated by arrow. (*b4*) Higher magnification of region B4 (panel *b1*), a region where the cut of the nuclear envelope is between tangential and transverse; one pore, arrow, is cone-shaped while others are similar to those in *b3*. (*c*) Bar graph summarizing results with the pan-catalytic subunit antibody. Particle counts for the representative section (panel *b1*), light bars, and for the total area studied and documented with photographs (dark bars ± SD). Regions identified are the non-nuclear (*NN*) regions, the nuclear (*N*) regions, the outer membrane of the nuclear envelope (*ONM*), the inner membrane of the nuclear envelope (*INM*), regions where the nuclear envelope is cut tangentially (*E*), the sum of *INM* and *E* (*NE*) and the nucleoplasm (*NP*). Bars, panels *a1*, and *b1*, 1 μm; bars, all other panels, 0.5 μm.

PBFI (free dye) with K^+ (Fig. 4*b*, *empty squares*). Again, this provides significant validation for the experimental design employed.

There is clearly ATP-dependent, ouabain-sensitive maintenance of Na^+ and K^+ gradients between nuclear envelope lumen and nucleoplasm as well as nuclear envelope lumen and medium (cytoplasm). It is also clearly evident that these results are most consistent with Na,K-ATPase orientation in which the catalytic site is present in the nucleoplasm, since the addition of exogenous ATP (representing the extranuclear ATP stores that maintain the nuclear ATP pools (Rapaport, 1980)) caused an increase in the normalized SBFI fluorescence and a decrease in the normalized PBFI fluorescence. The steady-state lumenal Na^+ and K^+ concentrations are presented as ranges (Table 4); the ranges for Na^+ are more certain than the ranges for K^+. SBFI has a Na^+: K^+ selectivity of 20 and an effective K_d for Na^+, in the presence of K^+, of 20 mM (Minta & Tsien, 1989). This means that the values at low Na^+ concentrations (in this case, those in the presence of ouabain) are more accurate than those at Na^+ concentrations ≥ 60 mM, where the fluorescence ratio is approaching its limiting value. On the other hand, the values for the lumenal K^+ concentrations are less certain, as reflected in the stated estimates, since the K^+: Na^+ selectivity is 2. In spite of this caveat, the K^+ gradient does exist, because ouabain's effect on the ratio for PBFI was opposite that for SBFI.

Na,K-ATPase in the Nucleus and Plasma Membrane

Immunocytochemistry and immunostaining of Western blots were used to confirm the presence of Na,K-ATPase in the plasma membrane and nuclei of cultured HepG2 cells, in the plasma membrane and nuclei of hepatocytes in rat liver sections, as well as in isolated rat liver nuclei (Figs. 5–7). In HepG2 cells (Fig. 5*a*), Na,K-ATPase is present in the plasma membrane (punctate fluorescence on the cell surface) and in the nuclear envelope (arrows) of all of the cells in the field. The fluorescence intensity in the plasma membrane and nucleus was significantly lower when the affinity-purified preimmune serum (Fig. 5*b*), the IgG fraction of normal rabbit serum (*data not included*) or the IgG fraction isolated from the preabsorbed antiserum were used in place of the affinity-purified antibody. In isolated rat liver nuclei (Fig. 5*c*), Na,K-ATPase is evident in the nuclear envelope. Once again, when either affinity-purified preimmune serum, the IgG fraction of normal rabbit serum, or the IgG fraction of preabsorbed antiserum replaced the affinity-purified antibody, the fluorescence intensity was significantly decreased (Fig. 5*e*).

The data with immunostained western blots (Fig. 5*g*) are in agreement with the indirect immunofluor-

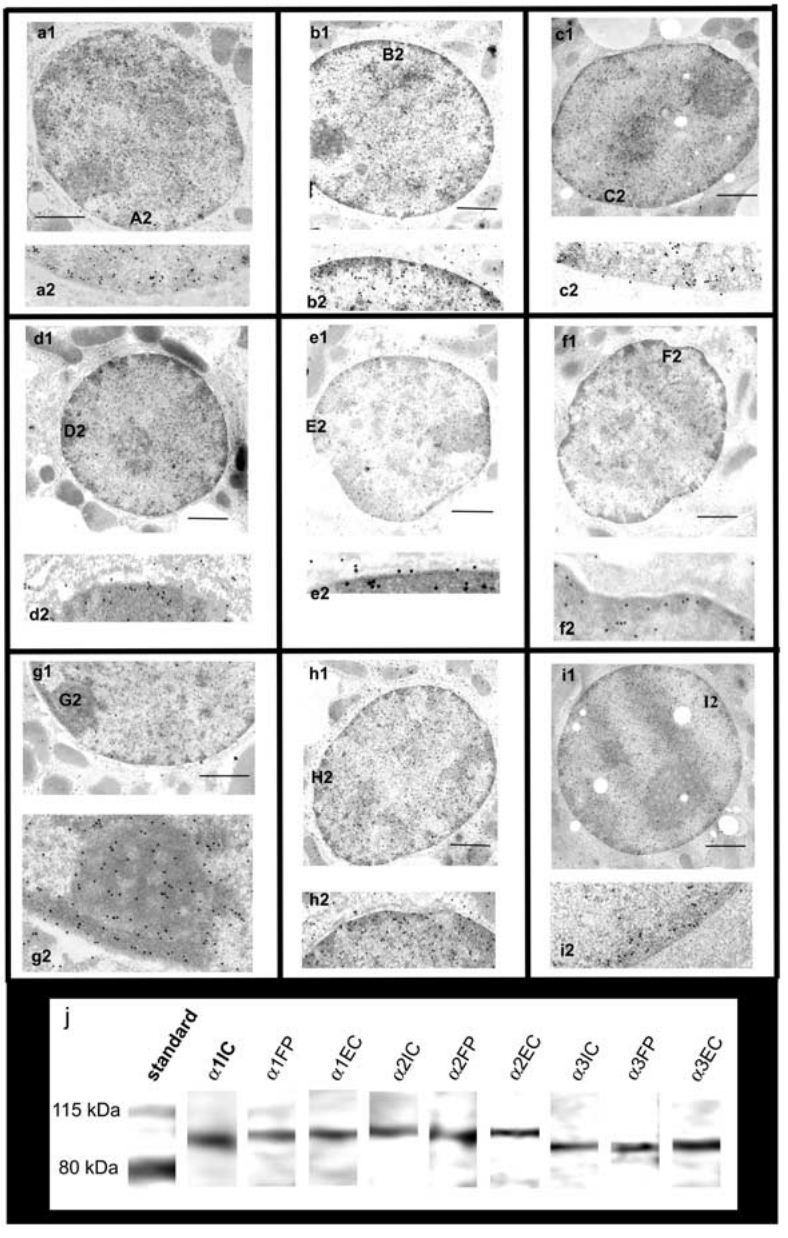

Fig. 7. Detection of Na,K-ATPase catalytic subunit isoforms in the nuclear envelope by immunogold electron microscopy. (*a1*) Representative micrograph of a liver section stained with affinity-purified α1IC; (*a2*) higher magnification of region designated *A2* in panel *a1*. (*b1*) Representative micrograph of a liver section stained with affinity-purified α1EC; (*b2*) higher magnification of region designated *B2* in panel *b1*. (*c1*) Representative micrograph of a liver section stained with affinity-purified α1FP; (*c2*) higher magnification of region designated *C2* in panel *c1*. (*d1*) Representative micrograph of a liver section stained with affinity-purified α2IC; (*d2*) higher magnification of region designated *D2* in panel *d1*. (*e1*) Representative micrograph of a liver section stained with affinity-purified α2EC; (*e2*) higher magnification of region designated *E2* in panel *e1*. (*f1*) Representative micrograph of a liver section stained with affinity-purified α2FP; (*f2*) higher magnification of region designated *F2* in panel *f1*. (*g1*) Representative micrograph of a liver section stained with affinity-purified α3IC; (*g2*) higher magnification of region designated *G2* in panel *g1*. Note that the envelope has been cut transversely so that nuclear pores are evident. (*h1*) Representative micrograph of a liver section stained with affinity-purified α3EC; (*h2*) higher magnification of region designated *H2* in panel *h1*. (*i1*) Representative micrograph of a liver section stained with affinity-purified α3FP; (*i2*) higher magnification of region designated *I2* in panel *i1*. (*j*) Representative results for staining of western blots of SDS-PAGE separations of the nuclear envelope preparation (liver nuclei) stained with the nine affinity-purified catalytic subunit isoform-specific antibodies. Bars represent 1.21 μm.

escence data. The affinity-purified anti-Na,K-ATPase antibody, αpan, (directed to the C-terminus of the catalytic subunits) stained a band (MW ~ 110 kDa) in rat liver nuclei preparations (Fig. 5*g*, lanes 1-4) and in microsomal preparations from rat heart, rat brain and rat kidney (Fig. 5*g*, lanes 5, 6, and 7, respectively). Immunoprecipitation was used to further confirm the presence of Na,K-ATPase in the membrane(s) of the nuclear envelope. When the αpan antibody was used to immunoprecipitate Na,K-ATPase from the rat liver nuclei preparation and the rat kidney microsomal preparation, a monoclonal antibody, specific for the α1 catalytic subunit (McDonough et al., 1996), stained bands (110 kDa) in both immunoprecipitates (Fig. 5*g*, lanes 8 and 9 for nuclei and renal microsomes, respectively).

Immunogold electron microscopy was used to test the hypothesis that arose from the fluorescent indicator studies, i.e., that the nuclear Na,K-ATPases are predominantly found in the nuclear envelope's inner membrane. As described below, the immunogold results confirm the localization of Na,K-ATPases to the inner membrane, especially in heterochromatin-rich areas (Fig. 6). In liver sections stained with preabsorbed antisera (Fig. 6*a1*,*a2* are representative micrographs), the number of gold particles per μm^2 was 12 ± 10 and 8 ± 7 for nuclear and non-nuclear regions, respectively. In liver sections stained with the affinity-purified αpan antibody, there was significantly more Na,K-ATPase in the nucleus (*N*) than in the nonnuclear regions (*NN*) (demonstrated under the appropriate headings in the bar

graph, Fig. 6*c*). As evident at higher magnification (Fig. 6*b2*), there was little Na,K-ATPase staining associated with the outer membrane of the nuclear envelope. Based on the results from a previous study of a nuclear pore protein (Nup116p), the 30-nm area from nuclear envelope center into the cytoplasm is the region in which complexes of gold-GAR(or Protein A)-primary antibody are to be expected when the antigen is in the outer membrane of the nuclear envelope (Bailer et al., 2000). Since the number of gold particles in the cytoplasm within 30 nm of the nuclear envelope's center (Fig. 6*c*, *ONM*) was not significantly different from the number in the non-nuclear regions, the nuclear envelope Na,K-ATPases are not concentrated in the outer membrane. Gold particles were present on the nucleoplasmic face of the nuclear envelope, associated with the heterochromatin material along the envelope's inner membrane (Fig. 6*b2*). Furthermore, the particle count per μm^2 in the area extending 30 nm from the center of the nuclear envelope lumen into the heterochromatin (Fig. 6*c*, *INM*) was significantly greater than that of the *ONM*, *NN*, *N* and *NP* (nucleoplasm) ($p \leq 0.05$). The nuclear pores were devoid of heterochromatin and gold particles. These observations are further substantiated by analysis of those areas of the micrograph where the nuclear envelope is sectioned tangentially (Fig. 6*b3* and *b4*; *a3* and *a4* are comparable regions in the control). In these areas, heterochromatin is evident below the envelope, punctuated by relatively heterochromatin-free regions 60–70 nm in diameter (i.e., the nuclear pores; Fig. 6*b3* and *b4*, *a3* and *a4*). The gold-particle counts in tangentially-sectioned regions, of which *b3* and *b4* are representative (designated *E* in the bar graph, Fig. 6*c*), are not statistically different from those for the *INM* but are significantly higher than the *NN*, *N*, ONM and *NP* ($p \leq 0.05$). Recent studies have demonstrated deep invaginations of the nuclear envelope (Fricker et al., 1997; Lui et al., 1998a) with associated heterochromatin. Several such invaginations are evident in the representative nucleus shown (Fig. 6*b1*) and have gold particles associated with them.

Immunogold electron microscopy with the affinity-purified antibodies specific for individual catalytic subunit isoforms indicates the presence of α1, α2 and α3 isoforms in the nuclear envelope's inner membrane (Fig. 7; Table 5). In liver sections stained with any of the nine isoform-specific antibodies (Fig. 7*a1–a2*, *b1–b2* and *c1–c2* for affinity-purified α1-specific antibodies; panels *d1–d2*, *e1–e2*, *f1–f2* for affinity-purified α2-specific antibodies; panels *g1–g2, h1–h2* and *i1–i2* for affinity-purified α3-specific antibodies), gold particles were most prevalent in the region along the inner membrane of the nuclear envelope within 30 nm from the center of the nuclear envelope lumen into the heterochromatin (*INM*, Table 5). There was no significant difference between the particles within

Table 5. Particle counts (particles/μm^2) from immunoelectron microscopy with catalytic subunit isoform-specific antibodies

Region Antibody	NN	ONM	INM	NP
α*1IC*	8 ± 8	12 ± 13	103 ± 46[b,c]	31 ± 20[d]
α *1EC*	11 ± 8	18 ± 14	100 ± 44[b,c]	34 ± 8[d]
α *1FP*	17 ± 14	19 ± 19	91 ± 58[b,c]	22 ± 12[d]
α *2IC*	18 ± 7	25 ± 21	91 ± 19[b,c]	51 ± 13[d]
α *2EC*	14 ± 8	24 ± 17	81 ± 25[b,c]	48 ± 15[d]
α *2FP*	14 ± 11	15 ± 8	91 ± 34[b,c]	13 ± 4
α *3IC*	12 ± 13	12 ± 13	103 ± 66[b,c]	31 ± 20[d]
α *3EC*	11 ± 6	18 ± 14	100 ± 44[b,c]	34 ± 8[d]
α *3FP*	12 ± 10	19 ± 19	91 ± 58[b,c]	22 ± 12[d]
Control[a]	12 ± 2	15 ± 14	23 ± 23	6 ± 4

[a]Since there was no statistical difference between preabsorbed, preimmune and rabbit serum IgG fractions, all have been included as controls ($n = 98$). $n = 32$ for antisera.
[b]Significantly different from the control ($p < 0.0001$; Mann Whitney).
[c]Significantly different from the NN and ONM values $p < 0.0001$; Mann Whitney).
[d]Significantly different from NN value for same antiserum ($p \leq 0.01$; Mann Whitney).

30 nm from the center of the nuclear envelope lumen into the cytoplasm (*ONM*) and non-nuclear regions (*NN*) with any of the affinity-purified isoform-specific antibodies. These results confirm those obtained with the pan-catalytic subunit antiserum (Fig. 6). With all antibodies except the anti-α2FP, there was a statistically significant difference between gold-particle counts in the nucleoplasm (*NP*) and non-nuclear (*NN*) regions. This result differs from that observed with the pan-catalytic subunit antiserum, probably reflecting the fact that the tangential regions (Fig. 7*g2*, for example) were not excluded in the *NP* counting with the isoform-specific antibodies. There were no tangential areas in the micrographs for the α1FP antibody. Aside from the nucleus, the α1-specific antibodies stained the canalicular and sinusoidal plasma membranes (*data not included*), a result similar to previously published studies (Simon et al., 1995, 1996). No plasma membrane staining was evident with the α2- and α3-specific antibodies.

To substantiate the immunogold results, immunoblot analysis was performed using purified liver nuclear envelopes and the nine affinity-purified catalytic-subunit isoform-specific antibodies. The results, Fig. 7*j*, demonstrate the presence of all three catalytic subunit isoforms in the nuclear envelope preparation. It should be pointed out at this time, that similar immunoblot experiments with the liver microsomal fraction (discussed previously in Table 1) showed staining with the three α1-specific antibodies and no staining with the α2- and α3-specific antibodies (*data not included*).

The immunogold results explain why the relatively membrane-impermeable ouabain was able to elicit changes in nucleoplasmic and lumenal Na^+ and

Table 6. Summary of findings

1. The lumenal Na^+ concentration is greater than that of the nucleoplasm.
2. The lumenal Na^+ concentration is greater than that of the cytoplasm.
3. The nucleoplasmic Na^+ concentration is less than that of the cytoplasm.
4. *In the presence of ouabain*, the lumenal Na^+ concentration approaches that of the cytoplasm and the nucleoplasmic Na^+ level remains less than that of the cytoplasm.
5. The lumenal K^+ concentration is less than that of the nucleoplasm.
6. The lumenal K^+ concentration is less than the cytoplasmic K^+ concentration.
7. The nucleoplasmic K^+ concentration is greater than that of the cytoplasm.
8. *In the presence of ouabain*, the lumenal K^+ concentration increases while the nucleoplasmic K^+ concentration remains greater than that of the cytoplasm.
9. Ouabain-sensitive Na, K-ATPases are located in the inner membrane of the nuclear envelope, with the catalytic site in the nucleoplasm.
10. The net Na^+ and K^+ permeability of the nuclear pore is regulated.

K^+ levels. If the α1 isoform were the only one present, the transport and cation indicator results would have been equivocal due to insufficient inhibitor levels. The rat α1 isoform has a relatively low affinity for ouabain (Noel et al., 1990). It takes approximately 1–2 mM ouabain to inhibit Na,K-ATPase containing the α1 subunit. Furthermore, the membrane permeability of ouabain is relatively low (Mercer & Dunham, 1981) so that the effective ouabain concentration was probably less than the bathing solution's 0.1 mM. The other rat catalytic subunit isoforms have much higher ouabain affinities (Dzimiri et al., 1987; Noel et al., 1990). In spite of the low membrane permeability, sufficient inhibitor was present in the nuclear envelope lumen to inhibit the α2 and α3 isoforms, since ouabain consistently caused changes in the radioisotope and monovalent cation experiments.

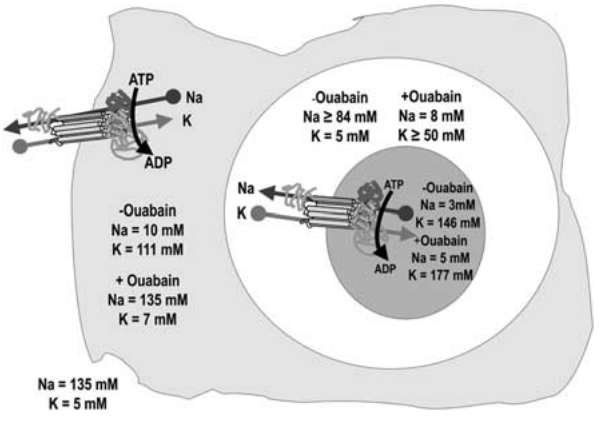

Fig. 8. Model of active sodium and potassium transport in the rat hepatocyte. Na, K-ATPase is present in the plasma membrane to support the transport of Na^+ out of and K^+ into the cell against steep trans-plasma membrane Na^+ and K^+ gradients. Na,K-ATPase is present in the inner membrane of the nuclear envelope to support the transport of Na^+ out of and K^+ into the nucleoplasm against steep trans-inner envelope membrane Na^+ and K^+ gradients. The energy derived from Na,K-ATPase-dependent ATP hydrolysis is required for the uphill transport of both monovalent cations across the plasma membrane and the inner membrane of the nuclear envelope. Ouabain inhibition of the plasma membrane or nuclear Na,K- ATPases causes dissipation of the monovalent cation gradients between cytoplasm and extracellular space or between nuclear envelope lumen and nucleoplasm/cytoplasm, respectively.

Discussion

Summary of Findings

This is the first report to suggest Na,K-ATPase regulation of nuclear monovalent cation concentrations. From the results of the experiments presented in this report, ten conclusions about Na^+ and K^+ regulation by Na,K-ATPases of the inner membrane of rat liver nuclei are evident (Table 6; Fig. 8). Essentially these results suggest that the Na^+ and K^+ concentrations of the nuclear envelope lumen can approximate those of extracellular space (high Na^+, low K^+) while the two compartments on either side of the envelope (cytoplasm and nucleoplasm) have low Na^+ and high K^+ concentrations.

Comparison of Results to Previous Studies

These results, although clear-cut, represent a paradigm shift that leads to the question, '*Why is this the first report of nuclear Na,K-ATPase?*' After all, Na,K-ATPase is the prototypical plasma membrane protein. Measurement of Na,K-ATPase activity is a classic method to demonstrate the presence or absence of plasma membrane contamination in other subcellular membrane fractions and/or organelles (Fleischer & Kervina, 1974). Furthermore, there are at least eighty-four published immunocytochemistry studies that support the concept of plasma membrane localization, eight of which are representative and will be used in the discussion to follow (Schenk, Hubert & Leffert, 1984; Takada et al., 1992; Simon et al., 1995, 1996; Zahler et al., 1996; Arystarkhova et al., 1999; Garner & Kong, 1999; Mobasheri, 1999). There are also several studies that have used immunogold to localize Na,K-ATPase in rat liver (Simon et al., 1995, 1996). Again, immunogold labeling of the nucleus was not reported in these studies. Finally, there is a growing number of studies with sodium green and SBFI, none of which report

nuclear sodium gradients (Donoso et al., 1992; Rose et al., 1999). Before discussing the significance of the present results, potential reasons for the apparent discrepancy between this study and the previous studies must be addressed.

First, antigen : antibody interactions depend upon antigen accessibility. This is especially critical for immunocytochemistry because of issues such as membrane permeability of the antibody and masking of the antigenic determinant(s) by cellular protein-protein interactions. It is generally accepted that permeabilization of fixed tissue is necessary for successful immunostaining of intracellular antigenic determinants. In fact, tissue permeabilization is commonly employed for immunocytochemistry of nuclear proteins, nuclear pore proteins and nuclear envelope proteins (Gee et al., 1997; Shah et al., 1998; Bailer et al., 2000). Since seven of the ten antisera used in the present study recognize intracellular epitopes of the Na,K-ATPase, 0.05–0.1% Triton X-100 was present in all solutions for immunocytochemistry, with the exception of the fixative solutions. Previous immunocytochemistry studies of liver hepatocytes have demonstrated Na,K-ATPase in the apical (canalicular) and basolateral (sinusoidal) membranes (Simon et al., 1995, 1996). Our data (not included in the present report) confirm these previous results for the hepatocyte plasmalemma. Nuclear envelope Na,K-ATPase was not detected in these (and many other) previous studies, most likely because tissue permeabilization was not employed.

In support of the assertion that detergent permeabilization is required to observe staining of the cell nucleus with Na,K-ATPase antibodies, we found three reports in which the tissue or cells were permeabilized to study Na,K-ATPase localization. In one of the three studies, observed perinuclear localization was considered a result of Brefeldin treatment of the tissue (Mobasheri, 1999). In another, nuclear staining was observed but attributed to nuclear autofluorescence due to nonspecific labeling with the secondary antibody (Zahler et al., 1996). In the third study, in which detergent permeabilization was used, the focus was colocalization of α- and γ-subunits in the distal convoluted tubule. In that study the magnification of the images, while appropriate for the presented results, was too low to assess subcellular localization (Arystarkhova et al., 1999).

Second, antigen : antibody interactions are also dependent upon the affinity of the antibody for the antigen as well as the stability of the antibody and/or antigenic determinant (i.e., protein conformational stability) under the experimental conditions used. Only one report was found that presented immunoblot analysis of the liver nuclear fraction with a Na,K-ATPase-specific antibody. No staining of the nuclear fraction and only weak staining of the homogenate were presented in that report (Khoo et al., 2000). This is not surprising, since the monoclonal antibody used in that study, clone 9-A5 (Schenk et al., 1984), was explicitly not recommended for Western Blot analysis by the manufacturer, although the usefulness of this antibody for immunocytochemistry, immunoprecipitation, and ELISA was indicated (Affinity Bioreagents, Golden CO, Catalog page G9). On the other hand, the polyclonal antisera used in the current study have been successfully used for immunocytochemistry, Western blot analysis, and immunoprecipitation. It is likely that antibody affinity or antigenic-determinant/antibody stability is the source of the discrepancy between the two reports.

The apparent discrepancy between the results with the monovalent cation indicators presented here and previously is most likely a result of experimental design differences. In the previous studies the focus was measurement of free monovalent cation concentrations in the cytoplasm. Currently, there is no method to deliver the monovalent cation indicators to specific subcellular organelles in whole-cell experiments. The experiments described in the present report utilized isolated nuclei.

Finally, it is possible that nuclear envelope Na,K-ATPases are not universal, i.e., common to all cells. Indeed, preliminary immunocytochemistry studies for the tissues of the eye (not included in the present report) indicate that the presence of nuclear envelope Na,K-ATPase is not general but is confined to distinct cell types.

Potential Significance of the Results

While this is the first report of sodium pump-generated Na^+ and K^+ gradients between nuclear envelope lumen : nucleoplasm and nuclear envelope lumen : cytoplasm (medium), others have reported Na^+ and K^+ gradients between nucleus and cytoplasm. The data from these previous studies, summarized in Fig. 9, were used to compute $[K^+]_{nuc} : [K^+]_{cyt}$ and $[Na^+]_{nuc} : [Na^+]_{cyt}$. In fresh *Bufo bufo* oocytes, the $[K^+]_{nuc} : [K^+]_{cyt}$ was determined to be 3.8; the $[Na^+]_{nuc} : [Na^+]_{cyt}$ was 1.0 (Dick, 1978). In cells of the cortical collecting duct of the rat kidney, $[K^+]_{nuc} : [K^+]_{cyt}$ was determined to be 1.16, 1.12 and 1.06 for the cortical thick ascending limb of Henle, principal cells and intercalated cells, respectively (Gifford et al., 1990). $[Na^+_{nuc}] : [Na^+_{cyt}]$ was determined to be $\sim$1.0 for the same three respective cell types (Gifford et al., 1990). In frog skin at extracellular pH values of 7.0 and 8.0, $[K^+]_{nuc} : [K^+]_{cyt}$ was determined to be 1.1, and $[Na^+]_{nuc} : [Na^+]_{cyt}$ was 1.0 (Rick, 1994).

What might be the function of nuclear monovalent cation gradients in normal and pathologic conditions? An early report of nuclear K^+ levels in *Chironomus* development (Wuhrmann et al., 1979)

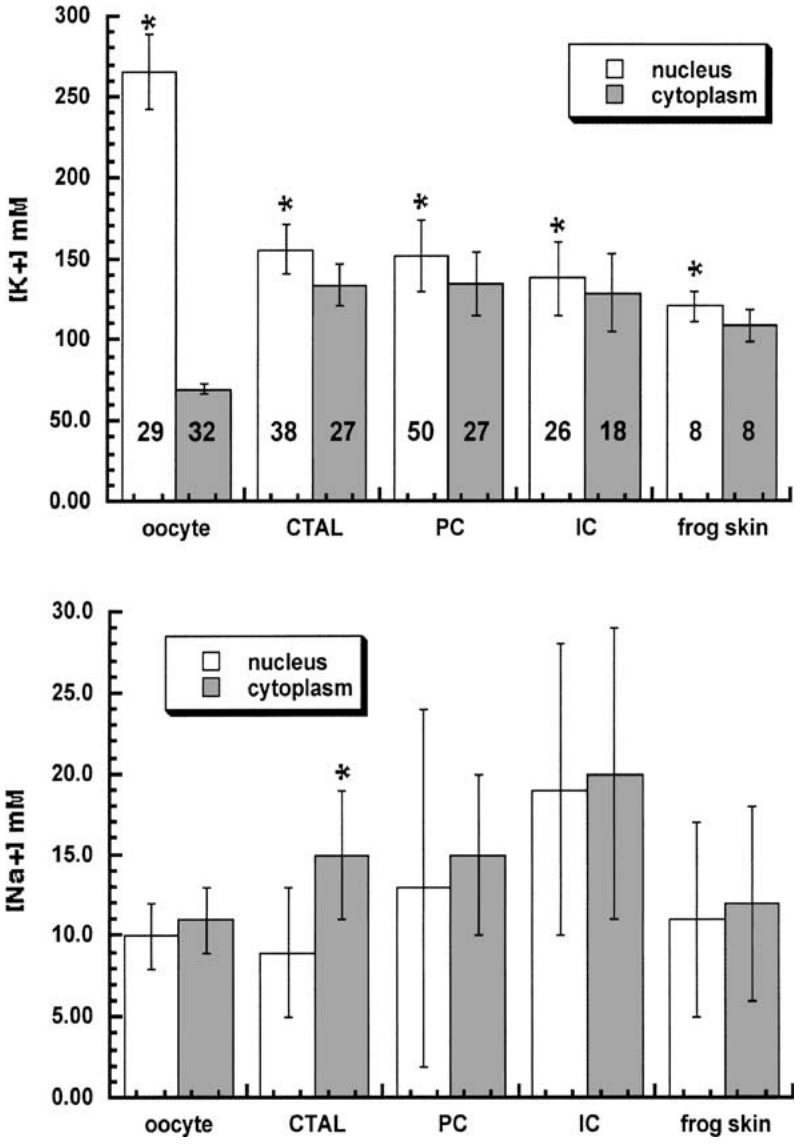

Fig. 9. Previously reported values for nuclear and cytoplasmic $[K^+]$ and $[Na^+]$. Nuclear (white bars) and cytoplasmic (grey bars) K^+ (top panel) and Na^+ (bottom panel) levels determined previously for oocytes (Dick, 1978), rat kidney cortical collecting ducts (CTAL, cortical thick ascending limb of Henle; PC, principal cells and IC, intercalated cells) (Gifford et al., 1990), and frog skin (Rick, 1994). Asterisks indicate those comparisons (nucleus : cytoplasm) where the differences in the values were considered significant ($p < 0.05$) by the authors. The numbers inside the bars of the top panel indicate the number of samples tested (N values). The sample sizes indicated for the K^+ measurements are the same for the Na^+ measurements.

may augur the importance of nuclear Na,K-ATPase-dependent Na^+/K^+ exchange to nuclear function. In the dormant oligophase of *Chironomus* development, nuclear K^+ was determined to be 12 ± 2 mg/g. In the prepupal phase of *Chironomus* development, a period of dramatic differentiation, there was a 1.5-fold increase in nuclear $[K^+]$. Concurrent with the increase in nuclear $[K^+]$ in the prepupal phase of *Chironomus* development, puffing or expansion of specific salivary chromosome regions was observed (Wuhrmann et al., 1979).

While there is no direct evidence that changes in nuclear $[K^+]$ or $[Na^+]$ regulate DNA structure in vivo, there are compelling in vitro data to suggest a role for monovalent cations in the regulation of DNA structure as well as regulation of interactions between DNA and DNA-binding proteins. DNA's high axial charge requires stabilization by electrostatic interactions with counterions; i.e., DNA can be viewed as a cation exchanger. Counterions that compete with one another for electrostatic interaction with nucleic acids include NH_4^+, K^+, Na^+, Li^+, Cs^+, Mg^{2+} and Ca^{2+}, as well as the positively charged amino-acid side chains of specific domains of DNA binding proteins. It is well established that increasing the monovalent cation concentration elevates the melting temperature (T_M) of DNA; (Schildkraut, 1965; Blake & Delcourt, 1998). Monovalent cations primarily affect the structure of the minor groove (Jing et al., 1997; Bouaziz, Kettani & Patel, 1998; Kettani et al., 1998; McFail-Isom, Sines & Williams, 1999). K^+ is more effective than Na^+ at stabilizing G4 DNA, a structure that is believed to arrest DNA synthesis (Sen & Gilbert, 1992). Since G4 DNA structures arise in regions with G-rich motifs, it is not surprising that telomeric DNA structure is regulated and stabilized by monovalent cations in vitro (Williamson, Raghuraman & Cech, 1989; Sen & Gilbert, 1992; Guo,

Lu & Kallenbach, 1993; Choi & Choi, 1994; Miura, Benevides & Thomas, 1995; Schultze et al., 1999). In addition to direct effects on DNA structure, monovalent cations have been shown to affect interactions between several nuclear proteins and DNA (Fogolari et al., 1997; Ozers et al., 1997; Hamilton, Borel & Romaniuk, 1998; Roxstrom et al., 1998; Cherny et al., 1999; Winston et al., 1999).

From these examples as well as numerous other studies that, due to space limitations, were not cited, a hypothesis can be proposed that nuclear monovalent and divalent cation regulation is, at times, required for nuclear structure and function. Furthermore, since the Na,K-ATPase and the IP_3-regulated Ca^{2+}-channels are in the inner membrane of the nuclear envelope, regions rich in heterochromatin, it is likely that these cations are critical for the stabilization and destabilization of higher-order chromosome structure. Future studies will be necessary to test these hypotheses.

I thank Dr. M. Payne for his careful evaluation of this study and for his patiently prepared, constructive critiques of the numerous revisions of this report. I thank Dr. G. Sachs for his advice during the study and Dr. L. Oakford and Ms. A.-M. Brun-Zinkernagel for their assistance with the electorn microscopy and immunofluorescence. This research was supported by the National Eye Institute of the National Institutes of Health (EY07010).

References

Arystarkhova, E., Wetzel, R.K., Asinovski, N.K., Sweadner, K.J. 1999. The gamma subunit modulates Na(+) and K(+) affinity of the renal Na,K-ATPase. *J. Biol. Chem.* **274:**33183–33185

Bachs, O, Agell, N., Carafoli, E. 1994. Calmodulin and calmodulin-binding proteins in the nucleus. *Cell Calcium* **16:**289–296

Bailer, S.M., Balduf, C., Katahira, J., Podtelejnikov, A., Rollenhagen, C., Mann, M., Pante, N., Hurt, E. 2000. Nup116p associates with the Nup82p-Nsp1p-Nup159p nucleoporin complex. *J. Biol. Chem.* **275:**23540–23548

Blake, R.D., Delcourt, S.G. 1998. Thermal stability of DNA. *Nucleic Acids Res.* **26:**3323–3332

Blanco, G., Mercer, R.W. 1998. Isozymes of the Na-K-ATPase: heterogeneity in structure, diversity in function. *Am. J. Physiol.* **275:**F633–650

Bouaziz, S., Kettani, A., Patel, D.J. 1998. A K cation-induced conformational switch within a loop spanning segment of a DNA quadruplex containing G-G-G-C repeats. *J. Mol. Biol.* **282**:637–652

Bustamante, J.O. 1992. Nuclear ion channels in cardiac myocytes. *Pfluegers Arch.* **421:**473–485

Bustamante, J.O., Hanover, J.A., Liepins, A. 1995. The ion channel behavior of the nuclear pore complex. *J. Membrane Biol.* **146:**239–251

Cherny, D.I., Striker, G., Subramaniam, V., Jett, S.D., Palecek, E., Jovin, T.M. 1999. DNA bending due to specific p53 and p53 core domain-DNA interactions visualized by electron microscopy. *J. Mol. Biol.* **294:**1015–1026

Choi, K.H., Choi, B.S. 1994. Formation of a hairpin structure by telomere 3′ overhang. *Biochim. Biophys. Acta* **1217:**341–344

Crambert, G., Hasler, U., Beggah, AT., Yu, C., Modyanov, N.N., Horisberger, J.D., Lelievre, L, Geering, K. 2000. Transport and pharmacological properties of nine different human Na,K-ATPase isozymes. *J. Biol. Chem.* **275:**1976–1986

Dick, D.A. 1978. The distribution of sodium, potassium and chloride in the nucleus and cytoplasm of Bufo bufo oocytes measured by electron microprobe analysis. *J. Physiol.* **284:**37–53

Donoso, P., Mill, J.G., O'Neill, S.C., Eisner, D.A. 1992. Fluorescence measurements of cytoplasmic and mitochondrial sodium concentration in rat ventricular myocytes. *J. Physiol.* **448:**493–509

Dwyer, N., Blobel, G. 1976. A modified procedure for the isolation of a pore complex-lamina fraction from rat liver nuclei. *J. Cell. Biol.* **70:**581–591

Dzimiri, N., Fricke, U., Klaus, W. 1987. Influence of derivation on the lipophilicity and inhibitory actions of cardiac glycosides on myocardial Na^+-K^+-ATPase. *Br. J. Pharmac.* **91:**31–38

Fleischer, S., Kervina, M. 1974. Subcellular fractionation of rat liver. *Methods Enzymol.* **31:**316–341

Fogolari, F., Elcock, A.H., Esposito, G., Viglino, P., Briggs, J.M., McCammon, J.A. 1997. Electrostatic effects in homeodomain-DNA interactions. *J. Mol. Biol.* **267:**368–381

Fricker, M., Hollinshead, M., White, N., Vaux, D. 1997. Interphase nuclei of many mammalian cell types contain deep, dynamic, tubular membrane-bound invaginations of the nuclear envelope. *J. Cell Biol.* **136:**531–544

Garner, M.H., Bahador, A., Thi Nguyen, B.T., Wang, R.R., Spector, A. 1992. Na,K-ATPase of cultured bovine lens epithelial cells: H2O2 effects. *Exp. Eye Res.* **54:**321–328

Garner, M.H., Horwitz, J. 1994. Catalytic subunit isoforms of mammalian lens Na,K-ATPase. *Curr. Eye Res.* **13:**65–77

Garner, M.H., Kong, Y. 1999. Lens epithelium and fiber Na,K-ATPases: distribution and localization by immunocytochemistry. *Invest. Ophthalmol. Vis. Sci.* **40:**2291–2298

Gee, S., Krauss, S.W., Miller, E., Aoyagi, K., Arenas, J., Conboy, J.G. 1997. Cloning of mDEAH9, a putative RNA helicase and mammalian homologue of *Saccharomyces cerevisiae* splicing factor Prp43. *Proc. Natl. Acad. Sci. USA* **94:**11803–11807

Gerasimenko, O.V., Gerasimenko, J.V., Tepikin, A.V., Petersen, O.H. 1995. ATP-dependent accumulation and inositol trisphosphate- or cyclic ADP-ribose-mediated release of Ca^{2+} from the nuclear envelope. *Cell* **80:**439–444

Gerasimenko, O.V., Gerasimenko, J.V., Tepikin, A.V., Petersen, O.H. 1996. Calcium transport pathways in the nucleus. *Pfluegers Arch.* **432:**1–6

Gifford, J.D., Galla, J.H., Luke, R.G., Rick, R. 1990. Ion concentrations in the rat CCD: differences between cell types and effect of alkalosis. *Am. J. Physiol.* **259:**F778–F782

Guihard, G., Proteau, S., Rousseau, E. 1997. Does the nuclear envelope contain two types of ligand-gated Ca^{2+} release channels? *FEBS Lett.* **414:**89–94

Guo, Q., Lu, M., Kallenbach, N.R. 1993. Effect of thymine tract length on the structure and stability of model telomeric sequences. *Biochemistry* **32:**3596–3603

Gurgueira, S.A., Meneghini, R. 1996. An ATP-dependent iron transport system in isolated rat liver nuclei. *J. Biol. Chem.* **271:**13616–13620

Hamilton, T.B., Borel, F., Romaniuk, P.J. 1998. Comparison of the DNA binding characteristics of the related zinc finger proteins WT1 and EGR1. *Biochemistry* **37:**2051–2058

Harb, J., Meflah, K., Duflos, Y., Bernard, S. 1983. Purification and properties of bovine liver plasma membrane 5′ nucleotidase. *Eur. J. Biochem.* **137:**131–138

Haugland, R.P. (1996) Handbook of Fluorescent Probes and Research Chemicals, 6th ed. Molecular Probes, Eugene, OR

Hubbard, A.L., Wall, D.A., Ma, A. 1983. Isolation of rat hepatocyte plasma membranes. I. Presence of the three major domains. *J. Cell Biol.* **96:**217–229

Jing, N., Gao, X., Rando, R.F., Hogan, M.E. 1997. Potassium-induced loop conformational transition of a potent anti-HIV oligonucleotide. *J. Biomol. Struct. Dyn.* **15:**573–585

Kettani, A., Bouaziz, S., Gorin, A., Zhao, H., Jones, R.A., Patel, D.J. 1998. Solution structure of a Na cation stabilized DNA quadruplex containing G.G.G.G and G.C.G.C tetrads formed by G-G-G-C repeats observed in adeno-associated viral DNA. *J. Mol. Biol.* **282:**619–636

Khoo, K.M., Han, M.K., Park, J.B., Chae, S.W., Km, U.H., Lee, H.C., Bay, B.H., Chang, C.F. 2000. Localization of the cyclic ADP-ribose-dependent calcium signaling pathway in hepatocyte nucleus. *J. Biol. Chem.* **275:**24807–24817

Lanini, L., Bachs, O., Carafoli, E. 1992. The calcium pump of the liver nuclear membrane is identical to that of endoplasmic reticulum. *J. Biol. Chem.* **267:**11548–11552

Lingrel, J.B., Arguello, J.M., Van Huysse, J., Kuntzweiler, T.A. 1997. Cation and cardiac glycoside binding sites of the Na,K-ATPase. *Ann. N. Y. Acad. Sci.* **834:**194–206

Lui, P.P., Kong, S.K., Kwok, T.T., Lee, C.Y. 1998a. The nucleus of HeLa cell contains tubular structures for Ca^{2+} signalling. *Biochem. Biophys. Res. Commun.* **247:**88–93

Lui, P.P., Lee, C.Y., Tsang, D., Kong, S.K. 1998b. Ca^{2+} is released from the nuclear tubular structure into nucleoplasm in C6 glioma cells after stimulation with phorbol ester. *FEBS Lett.* **432:**82–87

Marshall, I.C., Gant, T.M., Wilson, K.L. 1997. Ionophore-releasable lumenal Ca^{2+} stores are not required for nuclear envelope assembly or nuclear protein import in *Xenopus* egg extracts. *Cell Calcium* **21:**151–161

Maruyama, Y., Shimada, H., Taniguchi, J. 1995. Ca(2+)-activated K(+)-channels in the nuclear envelope isolated from single pancreatic acinar cells. *Pfluegers Arch.* **430:**148–150

Masuda, A., Oyamada, M., Nagaoka, T., Tateishi, N., Takamatsu, T. 1998. Regulation of cytosol-nucleus pH gradients by K^+/H^+ exchange mechanism in the nuclear envelope of neonatal rat astrocytes. *Brain Res.* **807:**70–77

Mazzanti, M., DeFelice, L.J., Cohn, J., Malter, H. 1990. Ion channels in the nuclear envelope. *Nature* **343:**764–767

McDonough, A.A., Zhang, Y., Shin, V., Frank, J.S. 1996. Subcellular distribution of sodium pump isoform subunits in mammalian cardiac myocytes. *Am. J. Physiol.* **270:**C1221–C1227

McFail-Isom, L., Sines, C.C., Williams, L.D. 1999. DNA structure: cations in charge? *Cuur. Opin. Struct. Biol.* **9:**298–304

Mercer, R., Dunham, P. 1981. Studies on membrane-bound glyco lytic enzymes on inside-out vesicles from human red cell membranes. *J. Gen. Phys.* **78:**547–568

Minta, A., Tsien, R.Y. 1989. Fluorescent indicators for cytosolic sodium. *J. Biol. Chem.* **264:**19449–19457

Miura, T., Benevides, J.M., Thomas G.J., Jr. 1995. A phase diagram for sodium and potassium ion control of polymorphism in telomeric DNA. *J. Mol. Biol.* **248:**233–238

Mobasheri, A. 1999. Brefeldin A influences the cell surface abundance and intracellular pools of low and high ouabain affinity Na+, K(+)-ATPase alpha subunit isoforms in articular chondrocytes. *Histol. Histopathol.* **14:**427–438

Neitcheva, T., Peeva, D. 1995. Phospholipid composition, phospholipase A2 and sphingomyelinase activities in rat liver nuclear membrane and matrix. *Int. J. Biol. Chem Cell Biol.* **27:**995–1001

Noel, F., Fagoo, M., Godfraind, T. 1990. A comparison of the affinities of rat (Na^+ + K^+)-ATPase isozymes for cardioactive steroids, role of lactone ring, sugar moiety and KCl concentration. *Biochem. Pharmacol.* **40:**2611–2616

Ozers, M.S., Hill, J.J., Ervin, K., Wood, J.R., Nardulli, A.M., Royer, C.A., Gorski, J. 1997. Equilibrium binding of estrogen receptor with DNA using fluorescence anisotropy. *J. Biol. Chem.* **272:**30405–30411

Rapaport, E. 1980. Compartmentalized ATP pools produced from adenosine are nuclear pools. *J. Cell Physiol.* **105:**267–274

Rick, R. 1994. pHi determines rate of sodium transport in frog skin: results of a new method to determine pHi. *Am. J. Physiol.* **266:**F367–F374

Rose, C.R., Kovalchuk, Y., Eilers, J., Konnerth, A. 1999. Two-photon Na^+ imaging in spines and fine dendrites of central neurons. *Pfluegers Arch.* **439:**201–207

Roxstrom, G., Velazquez, I., Paulino, M., Tapia, O. 1998. DNA structure and fluctuations sensed from a 1.1ns molecular dynamics trajectory of a fully charged Zif268-DNA complex in water. *J. Biomol. Struct. Dyn.* **16:**301–312

Santella, L., Kyozuka, K. 1997. Effects of 1-methyladenine on nuclear Ca^{2+} transients and meiosis resumption in starfish oocytes are mimicked by the nuclear injection of inositol 1,4,5-trisphosphate and cADP-ribose. *Cell Calcium* **22:**11–20

Schenk, D.B., Hubert, J.J., Leffert, H.L. 1984. Use of a monoclonal antibody to quantify (Na^+, K^+)-ATPase activity and sites in normal and regenerating rat liver. *J. Biol. Chem.* **259:**14941–14951

Schildkraut, C. 1965. Dependence of the melting of DNA on salt concentration and temperature. *Biopolymers* **3:**195–208

Schultze, P., Hud, N.V., Smith, F.W., Feigon, J. 1999. The effect of sodium, potassium and ammonium ions on the conformation of the dimeric quadruplex formed by the *Oxytricha nova* telomere repeat oligonucleotide d(G(4)T(4)G(4)). *Nucleic Acids Res.* **27:**3018–3028

Sehmi, D., Williams, L.G., Williams, D.J. 1986. Microsomal membrane subfractionation by a lectin affinity method. *FEBS Lett.* **197:**335–338

Sen, D., Gilbert, W. 1992. Novel DNA superstructures formed by telomere-like oligomers. *Biochemistry* **31:**65–70

Shah, S., Tugendreich, S., Forbes, D. 1998. Major binding sites for the nuclear import receptor are the internal nucleoporin Nup153 and the adjacent nuclear filament protein Tpr. *J. Cell. Biol.* **141:**31–49

Shyjan, A.W., Levenson, R. 1989. Antisera specific for the alpha 1, alpha 2, alpha 3, and beta subunits of the Na,K-ATPase: differential expression of alpha and beta sub-units in rat tissue membranes. *Biochemistry* **28:**4531–4535

Simon, F.R., Fortune, J., Alexander, A., Iwahashi, M., Dahl, R., Sutherland, E. 1996. Increased hepatic Na,K-ATPase activity during hepatic regeneration is associated with induction of the beta1-subunit and expression on the bile canalicular domain. *J. Biol. Chem.* **271:**24967–24975

Simon, F.R., Leffert, H.L, Ellisman, M., Iwahashi, M., Deerinck, T., Fortune, J., Morales, D., Dahl, R., Sutherland, E. 1995. Hepatic Na(+)-K(+)-ATPase enzyme activity correlates with polarized beta-subunit expression. *Am. J. Physiol.* **269:**C69–C84

Skou, J.C., Esmann, M. 1992. The Na,K-ATPase. *J. Bloenerg. Biomembr.* **24:**249–261

Strubing, C., Clapham, D.E. 1999. Active nuclear import and export is independent of lumenal Ca^{2+} stores in intact mammalian cells. *J. Gen. Physiol.* **113:**239–248

Szmacinski, H., Lakowicz, J.R. 1997. Sodium Green as a potential probe for intracellular sodium imaging based on fluorescence lifetime. *Anal. Biochem.* **250:**131–138

Tabares, L., Mazzanti, M., Clapham, D.E. 1991. Chloride channels in the nuclear membrane. *J. Membrane Biol.* **123:**49–54

Takada, T., Yamamoto, A., Omori, K., Tashiro, Y. 1992. Quantitative immunogold localization of Na,K-ATPase along rat nephron. *Histochemistry* **98:**183–197

Williamson, J.R., Raghuraman, M.K., Cech, T.R. 1989. Monovalent cation-induced structure of telomeric DNA: the G-quartet model. *Cell* **59:**871–880

Winston, R.L., Millar, D.P., Gottesfeld, J.M., Kent, S.B. 1999. Characterization of the DNA binding properties of the bHLH domain of Deadpan to single and tandem sites. *Biochemistry* **38:**5138–5146

Wuhrmann, P., Ineichen, H., Riesen-Willi, U., Lezzi, M. 1979. Change in nuclear potassium electrochemical activity and puffing of potassium-sensitive salivary chromosome regions during *Chironomus* development. *Proc. Natl. Acad. Sci. USA* **76:**806–808

Zahler, R., Gilmore-Hebert, M., Sun, W., Benz, E.J. 1996. Na,K-ATPase isoform gene expression in normal and hypertrophied dog heart. *Basic Res. Cardiol.* **91:**256–266